析の対象としたのは，US Environmental Protection Agency（EPA）に環境汚染物質として測定すべき項目としてリストアップされた16種類のPAHのうち，毒性の観点からヒトの健康に影響を及ぼし易いとされる4環以上の6種PAHを選択した．また，NPAHについては，特に変異原性が強いことが示されている11種を分析対象とした．その結果，大気中6種PAHの年平均濃度和は，撫順（1205 $pmolm^{-3}$）＞瀋陽（313 $pmolm^{-3}$）＞北京（270 $pmolm^{-3}$）＞鉄嶺（258 $pmolm^{-3}$）＞ウラジオストク（34 $pmolm^{-3}$）＞北九州（12 $pmolm^{-3}$）＞札幌（11 $pmolm^{-3}$）＞東京（5.9 $pmolm^{-3}$）＞釜山（5.6 $pmolm^{-3}$）＞金沢（3.6 $pmolm^{-3}$）の順となった．中国の都市のPAH, NPAHの年平均濃度は他国の都市に比して非常に高い値を計測した．近年，中国では発展する産業や冬季の暖房に多量の石炭を使用しているが，[1] 排煙脱粒子装置の普及は進んでいない．このため，PAHやNPAHが吸着した粒子状物質が多く排出されている．

3. 日本海域及び関連河川におけるPAH濃度

日本海域は，地震や火山活動の盛んな地帯であるとともに，タンカーやパイプライン等の事故の危険性も増している．[2,3] また中国等からの大気汚染の影響も受け易く，両端が狭い海峡で閉鎖性が高く環境変化に敏感である．したがって日本海の汚染調査は国際的にも要望されているものの，これまでその実態に関する報告はほとんどなかった．そこで筆者らは，日本海におけるPAH汚染の実態を把握すべく，海水中のPAH濃度測定を実施することとした．測定の対象は，人為起源汚染物質である3環から6環の合計13種のPAHとした．

総PAH濃度は，日本列島側，大陸側外洋域でそれぞれ，9.63 ng/L（3.44–24.0 ng/L），7.67 ng/L（4.10–30.6 ng/L）であり，大陸側がやや低かった．さらに，瀬戸内海や東北沿岸太平洋域の総PAH濃度と比較すると，日本海は瀬戸内海より低く，東北沿岸太平洋側外と同じレベルであったが，大西洋より数桁高かった．

今後，さらにデータを蓄積させることにより，汚染の現状はより明らかになっていくと考える．

4. PAH誘導体の生成

上で述べたように，発生したPAH類は発生源周辺に留まるに限らず，様々な要因により長距離を輸送され，輸送中に，PAHは紫外線やニトロラジカ

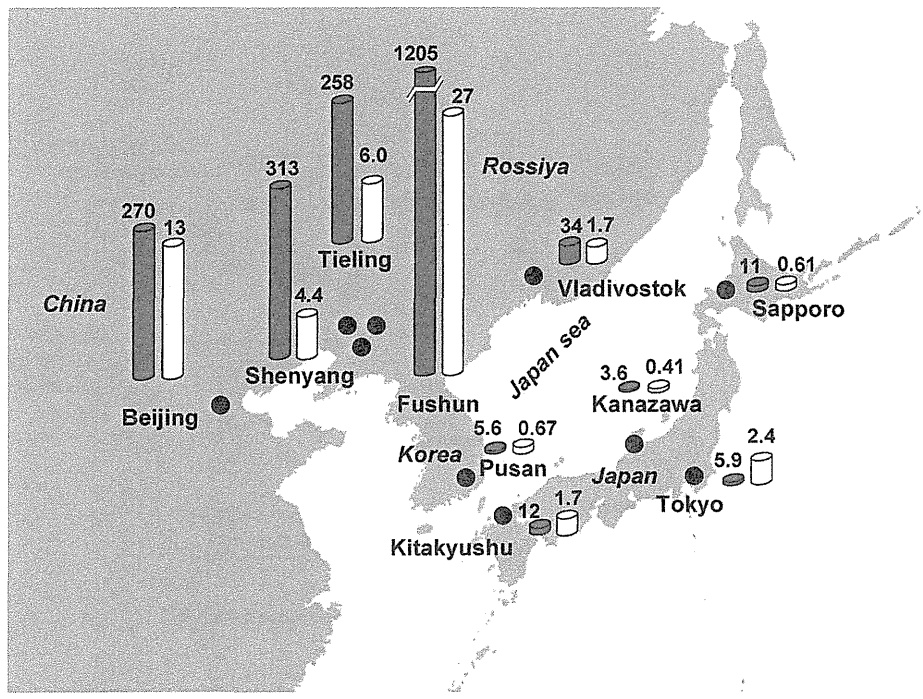

Fig. 1. Annual Average Atmospheric Concentrations of PAHs and NPAHs

Unit: pmol/m³ ■ [PAHs] = [Pyr] + [BaA] + [Chr] + [BbF] + [BkF] + [BaP], □ [NPAHs] = [1,3-Dnp] + [1,6-Dnp] + [1,8-Dnp] + [9-NA] + [1-NP] + [2-NFR1 + 2-NP] + [6-Nc] + [7-NBaA] + [6-NBaP] + [3-Nper], Year: 2001–2002 (Shenyang), 2002–2003 (Pusan), 2003–2004 (Tieling), 2004–2005 (Beijing, Fushun, Vladivostok, Kanazawa, Sapporo, Tokyo, Kitakyushu).

ル（$\cdot NO_3$），ヒドロキシラジカル（$\cdot OH$）などと化学反応すると，PAH ニトロ体（NPAH），PAH 水酸化体（PAHOH），PAH キノン体（PAHQ）等の誘導体となる.[4-6]

一方，これら PAH 誘導体は，生体内に取り込まれた後，代謝によっても生成する．例えば，PAH 類は，主に肝臓において，アリール炭化水素受容体（AhR）を活性化することにより薬物代謝酵素，CYP1A1 等のシトクロム P450 酵素などを誘導し，ついで P450 の存在下で PAH 類は PAHOH や PAHQ といった PAH 誘導体へと代謝される（Fig. 2）.[7]

5. PAH 誘導体による毒性影響

上で述べたように環境中に放出された PAH は PAH 誘導体となって存在しているため，PAH 誘導体が生体に対してどのような作用を示すかが重要となってくる．PAH 誘導体の毒性としては，NPAH による変異原性が古くからよく知られている．NPAH は，PAH がニトロ還元酵素（Nitroreductase: NTR）により代謝を受けることにより生成し，それらは最終的に DNA へ損傷を及ぼす付加体となることで，強い変異原性を示すことが知られている.[8] また，PAHQ についても活性酸素種（ROS）産生能を有すことから,[9] ラジカルの生成を経て物理的に DNA を損傷させ，細胞機能障害や細胞死を引き起こすことも知られている.[10-13] このような酸化ストレスは，多くの経路で，がんを始めとし，循環器系疾患，感染症，老化など様々な疾患に関与するとされる.[14]

一方で，近年，着目されているのが，PAH 誘導体による内分泌撹乱作用である．酵母 two-hybrid assay を用いた PAH 代謝産物によるエストロゲン受容体への作用を調べたわれわれの実験結果から，PAH 代謝産物である PAHOH 及び PAHQ がエストロゲン様/抗エストロゲン様作用を示すことが明らかとなっている.[15,16]

このように，大気中での様々な化学反応によって PAH 誘導体が生成するのと同時に，体内に取り込まれた PAH は，生体内の様々な代謝を介して無数の PAH 誘導体を生成することから，われわれは様々な生理活性作用を示す PAH 誘導体に高濃度曝露されている可能性が高い.

6. PAH 誘導体が示す構造活性相関

PAH 等の環境化学物質が示すエストロゲン受容体（ER）を中心としたホルモン受容体への結合及び活性化といった作用は，その立体構造によって，作用の有無や強弱が異なるものと推測される．そこで，PAHOH 及び PAHQ が示すエストロゲン/抗

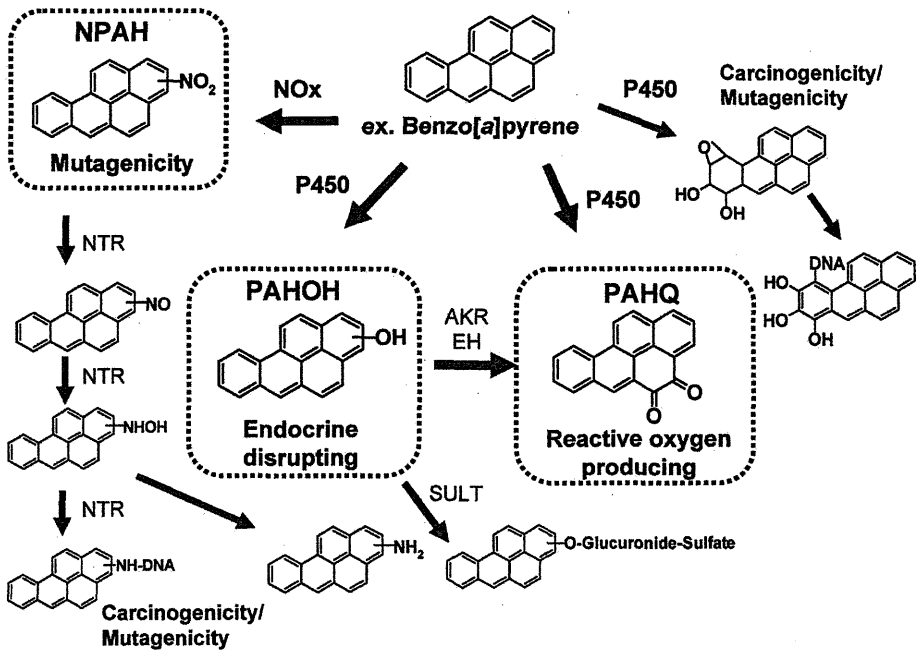

Fig. 2. Metabolic Activation of PAH/NPAH
NTR: Nitroreductase, AKR: Aldo-keto reductase, EH: Epoxide hydrase, SULT: Sulfotransferase.

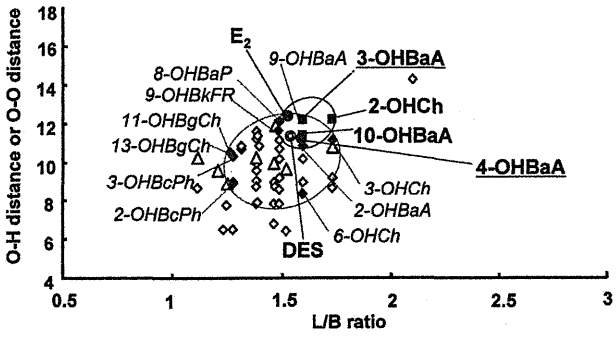

Fig. 3. Relatioship between L/B Ratios and O-H Distances of Strongly Estrogenic and Antiestrogenic PAHOHs

Estrogenic activity of each test compound was assayed in the concentration range from 1×10^{-6} M to 1×10^{-9} M. Reactive effective potency of estrogenic activity (REP_E) was calculated from the value of E_2 as a positive control. Antiestrogenic activity of each test compound was assayed in the concentration range from 1×10^{-6} M to 1×10^{-9} M. Reactive effective potency of antiestrogenic activity (REP_{AE}) was calculated from the value of 4-hydroxytamoxifen (4-OHT) as a positive control. Symbols: ■; Strong estrogenic activity ($REP_E\geq0.001$), ◆; Strong antiestrogenic activity ($REP_{AE}>0.1$), ◎; DES, ●; E2. In the case of E_2 and DES, O-O distance was used instead of O-H distance.[15]

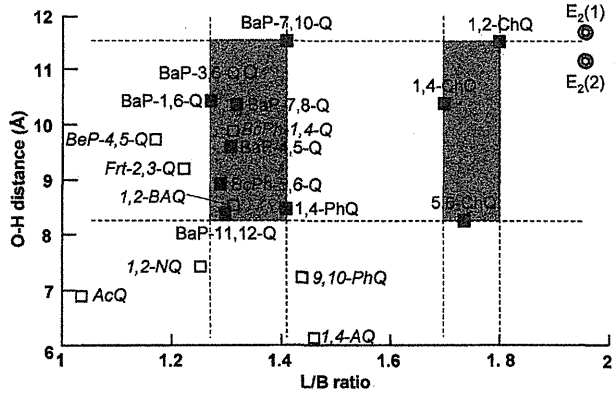

Fig. 4. Relatioship between L/B Ratios and O-H Distances of Strongly Estrogenic and Antiestrogenic PAHQs

Estrogenic activity of each test compound was assayed in the concentration range from 1×10^{-6} M to 1×10^{-9} M. Reactive effective potency of estrogenic activity (REP_E) was calculated from the value of E_2 as a positive control. Antiestrogenic activity of each test compound was assayed in the concentration range from 1×10^{-6} M to 1×10^{-9} M. Reactive effective potency of antiestrogenic activity (REP_{AE}) was calculated from the value of 4-hydroxytamoxifen (4-OHT) as a positive control. Symbols: ○; Estrogenic activity ($REP_E=2.3$), ■; Antiestrogenic activity ($REP_{AE}>0.42$), □; Inactive, ◎; E2.[16]

エストロゲン様作用について，分子構造又は物理化学的特性パラメーターによる予測が可能かどうか考察を行った．

われわれは，PAH の分子構造を考える上で 2 つの因子，すなわち，母核構造と水酸基の位置が活性に関与していることを予測し，母核構造の違いを表すパラメーターである Length-to-breadth ratio（L/B 比）[17,18] 及び水酸基の位置を表すパラメーターとして O-H distance[19] を使用した構造活性相関を調べた．

まず，PAHOH における活性と L/B 比及び O-H-distance との関係を Fig. 3 に示した．図に示したように，ER のアゴニスト活性を示した化合物は，L/B 比が 1.5–1.7, O-H distance が 10.8–11.7 Å の範囲に，また抗エストロゲン活性を持つ PAHOH は L/B 比が 1.2–1.7, O-H distance が 8.4–11.6 Å の範囲に集中することが明らかとなった．また，PAHQ についても同様に調べた結果を Fig. 4 に示した．エストロゲン様活性を示した PAHQ は，L/B 比が 1.2–1.4 及び 1.7–1.8, O-H distance が 8.2–11.5 Å の狭い範囲に集中して存在していた．これらは，ER の既知アゴニスト化合物である 17β-Estradiol（E_2）及び diethylstilbestrol（DES）と類似しており，これらは活性を強く示す要因の 1 つであると考えられた．

以上の結果により，バイオアッセイにより示された PAHOH 及び PAHQ が有するエストロゲン/抗エストロゲン作用を *in silico* での構造活性相関により予測できたことは，環境中や生体内に無数に存在する PAH 誘導体のリスクを知る上での有効な手法となることが期待できる．

7. おわりに

以上，PAH 誘導体を中心にわれわれ東アジアを取り巻く環境について述べたが，主要な大気汚染物質の 1 つである PAH 類は，PAH 誘導体へと姿を変えてわれわれ人類の健康を脅かしている危険性があり，今後も PAH 誘導体の毒性や環境中濃度等，動態を突きとめていかなくてはならない大きな環境問題であると思われる．

REFERENCES

1) BP Statistical Review of World Energy, 2004.
2) Lorre A., Point V., *Mar. Pollut. Bull.*, **52**, 560–571 (2006).
3) Lipiatou E., Tolosa I., Simó R., Bouloubassi I., Dachs J., Marti S., Sicre M. A., Bayona J. M., Saliot A., Albagés J., *Deepsea Res. II*, **44**, 881–905 (1997).
4) Vione D., Barra S., De Gennaro G., De Rienzo M., Gilardoni S., Perrone M. G., Pozzoli L., *Ann. Chim.*, **94**, 17–32 (2004).
5) Kameda T., Akiyama A., Toriba A., Tang N.,

Hayakawa K., *Sci. Technol.*, **45**, 3325–3332 (2011).
6) Atkinson R., Arey J., *Environ. Health Perspect.*, **102**, 117–126 (1994).
7) Shimada T., *Drug Metab. Pharmacokinet.*, **21**, 257–276 (2006).
8) Nagy E., Zeisig M., Kawamura K., Hisamatsu Y., Sugeta A., Adachi S., Moller L., *Carcinogenesis*, **26**, 1821–1828 (2005).
9) Motoyama Y., Bekki K., Chung S. W., Tang N., Kameda T., Toriba A., Taguchi K., Hayakawa K., *J. Health Sci.*, **55**, 845–850 (2009).
10) Biswas S., Seema A., Rahman I., *Biochem. Pharmacol.*, **71**, 551–564 (2006).
11) Stadtman E. R., Berlett B. S., *Chem. Res. Toxicol.*, **10**, 485–494 (1997).
12) Valavanidis A., Vlahogianni T., Dassenaki M., Scoullos M., *Ecotokicol. Environ. Saf.*, **64**, 178–189 (2006).
13) Stadtman E. R., Levine R. L., *Amino Acids*, **25**, 207–218 (2003).
14) Xia T., Kovochich M., Nel A., *Clin. Occup. Environ. Med.*, **5**, 817–836 (2006).
15) Hayakawa K., Onoda Y., Tachikawa C., Hosoi S., Yoshita M., Chung S. W., Kizu R., Toriba A., Kameda T., Tang N., *J. Health Sci.*, **53**, 562–570 (2007).
16) Hayakawa K., Bekki K., Yoshita M., Tachikawa C., Kameda T., Tang N., Toriba A., Hosoi S., *J. Health Sci.*, **57**, 274–280 (2011).
17) Sander L. C., Wise S. A., *NIST Special Publication*, **922** (1997).
18) Collantes E. R., Tong W., Welsh W. J., *Anal. Chem.*, **68**, 2038–2043 (1996).
19) Kihara H., Uchida N., Ikuta S., "Bunshikidoho," Kodansha Scientific, Tokyo, 1994.

analytical chemistry

Article

pubs.acs.org/ac

Determination of Benzo[*a*]pyrene-7,10-quinone in Airborne Particulates by Using a Chemiluminescence Reaction of Hydrogen Peroxide and Hydrosulfite

Ruibo Li,[†,‡,§] Takayuki Kameda,[‡] Akira Toriba,[‡] Kazuichi Hayakawa,*[,‡] and Jin-Ming Lin*[,§]

[†]State Key Laboratory of Chemical Resource Engineering, School of Science, Beijing University of Chemical Technology, Beijing 10029, China

[‡]Graduate School of Natural Science and Technology, Kanazawa University, Kakuma-machi, Kanazawa 920-1192, Japan

[§]Beijing Key Laboratory of Microanalytical Methods and Instrumentation, Department of Chemistry, Tsinghua University, Beijing 100084, China

ABSTRACT: An ultraweak chemiluminescence (CL) was observed when sodium hydrosulfite ($NaHSO_3$) reacts with hydrogen peroxide (H_2O_2) and was enhanced 70 times by adding 10 pmol benzo[*a*]pyrene-7,10-quinone (7,10-BaPQ). The CL reaction is fast, and it reached maximum intensity in 0.1 s, and then decayed to baseline in 3 s. Mechanism of $NaHSO_3$-7,10-BaPQ-H_2O_2 system were investigated by CL spectrum, radical scavengers and electron spin resonance (ESR). Hydroxyl radical ($^{\bullet}OH$), super oxide anion radical ($^{\bullet}O_2^-$), and sulfite radical ($^{\bullet}SO_3^-$) were generated in the $NaHSO_3$-7, 10-BaPQ-H_2O_2 system. Reduction of 7,10-BaPQ by $^{\bullet}O_2^-$ radical gave excited semiquinone, which showed strong CL emission when decayed to its ground state. Maximum CL emission wavelength was located at 440 nm, which may belong to the excited semiquinone. This CL system was developed as post column detection of high performance liquid chromatography for the determination of 7,10-BaPQ. Linearity ranged from 50 fmol to 20 pmol (R^2 = 0.9995) with limit of detection of 30 fmol (S/N = 3). The proposed method was used to determine 7,10-BaPQ in airborne particulates. Average atmospheric concentrations of 7,10-BaPQ in Kanazawa in December 2010 and Wajima in October 2007 were 2.0 and 1.6 pg/m^3, respectively.

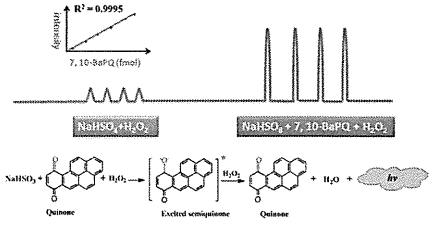

Polycyclic aromatic hydrocarbon (PAH) is an important class of environmental toxic organic compounds, which are formed by the burning of fossil fuels, industry waste, automobile exhausts, and tobacco smoke.[1−4] Degradation of PAHs leads to the generations of toxic derivatives, such as hydroxylated PAHs, nitro-PAHs, and PAH quinones.[5−8] PAH quinones are harmful environmental pollutants that induce the generation of reactive oxygen species (ROS) though their redox cycle in human body.[9−11] Many adverse health effects, such as aging, carcinogenesis, and inflammation, were related to the generations of ROS.[12,13] In addition, PAH quinones can combine with functional groups of enzymes to give covalent enzyme adducts, which can damage the activity of enzymes.[14,15] Furthermore, Hayakawa and co-workers have reported the estrogenic activity or antiestrogenic activity of PAH quinones.[16] Thus the health effects of PAHs and their derivatives became an important social concern. Therefore, it is necessary to establish a sensitive and reliable method to determine PAH quinones in the environment.

Gas chromatography mass spectrometry (GC-MS) has been reported as an efficient method to detect PAH quinones in airborne particulates. However, derivatization is necessary for GC-MS determination because of the high polarity and low vapor pressure of PAH quinones.[17] High performance liquid chromatography (HPLC) combined with atmospheric pressure ionization mass spectrometry (APCI-MS) is selective and sensitive for determination of PAH quinones.[18−21] In particular, tandem mass spectrometry (MS/MS) has been successfully applied to determine PAH quinones in airborne particulates. But the instrument is expensive for common use. Additionally, LC-MS/MS is not sensitive for four- and five-ring PAH quinones. HPLC with fluorescence detection was frequently used to determine PAHs and their derivatives. Unfortunately, most PAH quinones have no fluorescence emission. Thus, derivatization is needed for HPLC-fluorescence determination. Kishikawa and co-workers established several novel HPLC-fluorescence methods for determination of PAH quinones after derivatization.[22−24] These methods have high sensitivity and selectivity, but loss or contamination of analyte in the process of derivatization may affect accuracy of determination. The problem from derivatization was solved by Hayakawa and co-workers,[25] who combined a Pt−Rh catalytic column after separation column for reduction of PAH quinones. A strong fluorescence emission was observed after PAH quinone reduction. In the reported method,[25] PAH quinones can be detected online without derivatization. However, high cost and short lifetime of Pt−Rh catalytic column may limit the widespread use of the method. Chemiluminescence (CL) detection is a powerful method because excitation light is not needed compared with fluorescence detection. Low baseline signal of CL

Received: December 3, 2011
Accepted: February 27, 2012
Published: February 27, 2012

dx.doi.org/10.1021/ac2032063 | *Anal. Chem.* 2012, 84, 3215−3221

leads to higher sensitivity. HPLC with peroxyoxalate or luminol CL system with online post column ultraviolet irradiation was employed to determine PAH quinones with high selectivity and sensitivity.[26,27] But strict conditions make the methods not applicable for environmental samples.

In the present work, an ultrasensitive CL method for determination of 7,10-BaPQ based on $NaHSO_3$–H_2O_2 CL system was proposed. Although 7,10-BaPQ exhibits no fluorescence emission, a strong CL emission was observed when H_2O_2 was injected into $NaHSO_3$-7,10-BaPQ mixture solutions. 7,10-BaPQ can be detected without any derivatization or reduction in this method. Fmol level of 7,10-BaPQ can be determined easily. The proposed method was successfully applied to detect the concentrations of 7,10-BaPQ in airborne particulates for the first time.

EXPERIMENTAL SECTION

Chemicals and Reagents. Sodium hydrosulfite ($NaHSO_3$) and hydrogen peroxide (H_2O_2) were purchased from Kanto Chemical Co. Inc. (Tokyo, Japan). $NaHSO_3$ solution was freshly prepared by dissolving appropriate amount of $NaHSO_3$ powder in ultrapure water. H_2O_2 solution was freshly prepared by volumetric dilution of commercial 30% H_2O_2 solution. 7,10-BaPQ was obtained from NCI Chemical Carcinogen Repository (Kansas City, MO, U.S.A.). Nitro blue tetrazolium chloride (NBT) was purchased from Nacalai Tesque Inc. (Tokyo, Japan). 5, 5-Dimethyl-1-pyrroline-*N*-oxide (DMPO) was bought from Tokyo Kasei Kogyo Co. Ltd. (Tokyo, Japan). Thiourea and ascorbic acid were from Beijing Chemical Reagent, Co. (Beijing, China).

Solution of 7,10-BaPQ was prepared by dissolving powder with methanol. Standard solution of 7,10-BaPQ was diluted with methanol. All the organic solvents (methanol, hexane, dichloromethane, benzene, and ethanol) were HPLC grade from Wako Pure Chemical Industries, Ltd. Ultrapure water was obtained from a Milli-Q water purification system (Millipore, Bedford, MA, U.S.A.).

CL Profile and Emission Spectra. CL intensity versus time profile was measured by an ultraweak chemiluminescence analyzer (Institute of Biophysics, Chinese Academy of Science, Beijing, China). The signal was recorded by a computer with a data acquisition interface. Data acquisition and treatment were performed with BPCL software.

CL emission spectra were obtained in the same instrument as CL profile. Cutoff filters (400–640 nm), which were inserted between the cuvette and the PMT, were applied to measure the CL emission spectra.

HPLC. The separation of 7,10-BaPQ from samples was carried out on HPLC system as previously reported with some minor changes.[28] First, the separation column was changed to Waters AR-II 5C18 column (250 mm × 4.6 mm). CL detector was from Shimadzu Company (CLD-10A, Shimadzu, Kyoto, Japan). The flow rates of $NaHSO_3$, H_2O_2, and mobile phase were 2.0, 3.0, and 1.5 mL/min, respectively. Mobile phase was 80% (v/v) methanol in water.

LC-MS/MS. The Agilent 1100 series LC system consisted of a G1379A degasser, a G1312A binary pump, a G1367A auto sampler, and a G1316A column oven (all from Agilent Technologies, Palo Alto, CA). Separation of 7,10-BaPQ was performed on an Inertsil ODS-P column (250 mm ×4.6 mm, i.d.; 5.0 μm). The column temperature was kept at 30 °C. Mobile phase was 90% methanol at 0.5 mL/min in isocratic mode.

The mass spectrometric analyses were performed using an API 4000 Q-Trap tandem mass spectrometer (Applied Biosystems, Foster City, CA) equipped with an atmospheric pressure chemical ionization (APCI) source and operated in a positive ion mode. The ion-spay voltage was set to 5500 V. Nitrogen gas was used in all cases. Instrument setting were: curtain gas (10.0), nebulizer gas (10.0), collision gas (5.0). The collision energy was 35 eV. The source and probe temperatures were 30 and 400 °C, respectively. The mass spectrometer was operated under multiple reaction monitoring (MRM) mode, and monitoring ions were m/z 283 → 255 and 283 → 226.[21]

ESR Spectra. Electron spin resonance (ESR) spectra were measured on a JEOL spectrometer (JES-FA200, Japan). Instrument conditions: microwave frequency, 9.75 GHz, power, 12.72 mW, modulation amplitude, 2.01 G, modulation frequency, 100 kHz.

Sample Collection and Preparation. Airborne particulates were collected on the roof of a seven-storey building of Kanazawa University (Kakuma-machi) in Kanazawa, Japan. Wajima samples were collected in Wajima City in October, 2007. Sampling was conducted from November 28, 2010 to December 5, 2010 using a high-volume air sampler (Model 120, Kimoto Electrics, Osaka, Japan) with a 2500 QAT-UP quartz fiber filter (8 in. × 10 in., Pallflex Products, Putnam, CT, U.S.A.) at a flow rate of 1000 L/min (total volume 1434.9 m^3). Filter was changed every 24 h. The filters with airborne particulates were stored in a refrigerator at −20 °C until analysis.

Airborne particulates were extracted with the same method as previously reported with some small change.[28] First, in the previous work, whole filter was used. However, in this study, only half filter was needed. Second, the target compound 1-hydroxypyrene was eluted by 10 mL hexane/ethyl acetate in solid phase extraction step of the previous study, while

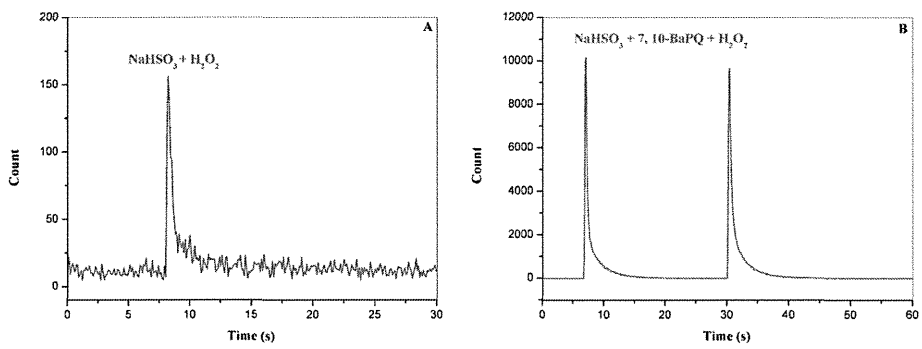

Figure 1. Observation of chemiluminescence emission. (A) $NaHSO_3$ solution was injected into H_2O_2 solution; and (B) $NaHSO_3$ solution was injected into H_2O_2–7,10-BaPQ mixture solutions. $NaHSO_3$, 0.1 mol/L; H_2O_2, 0.15 mol/L; injection volume, 100 μL.

dx.doi.org/10.1021/ac2032063 | *Anal. Chem.* 2012, 84, 3215–3221

dichloromethane was used to elute 7,10-BaPQ in the present work.

RESULTS AND DISCUSSION

CL Phenomenon. A batch CL system was used for the kinetic study of CL reaction. Figure 1A showed the kinetic curve of $NaHSO_3$–H_2O_2 CL reaction. $NaHSO_3$ reacted with H_2O_2 rapidly. An ultraweak CL emission which lasted less than 2s was observed when H_2O_2 was injected into $NaHSO_3$ (Figure 1A). CL intensity of $NaHSO_3$–H_2O_2 was increased 70 times after addition of 10 pmol 7,10-BaPQ (Figure 1B). However, the shape of kinetics curve of $NaHSO_3$–H_2O_2 was not changed by the addition of 7,10-BaPQ. No CL emission was observed when 7,10-BaQ was injected into with only $NaHSO_3$ or H_2O_2, which means 7,10-BaPQ can not react with only $NaHSO_3$ or H_2O_2. In addition, no signal was recorded when 7,10-BaPQ was injected into the mixture of $NaHSO_3$–H_2O_2 solution. One reason can explain this phenomenon. $NaHSO_3$ reacted with H_2O_2 in less than one second, when 7, 10-BaPQ was adding into the mixture, the reaction between $NaHSO_3$–H_2O_2 has finished.

Identification of the Radicals, Products, and Emitting Species in the CL System. To explain the CL phenomenon, radicals, emitting species, and products which were generated in the $NaHSO_3$–7,10-BaPQ–H_2O_2 CL system were investigated by radical scavengers, ESR spectrum, HPLC, and CL spectrum. The results were showed in Table 1 and Figures 2–4.

Table 1. Effect of Radical Scavengers on the $NaHSO_3$–7,10-BaPQ–H_2O_2 System[a]

radical scavengers	radical	concentration (mol/L)	CL intensity[b] of $NaHSO_3$–H_2O_2–7,10-BaPQ
without scavengers			1.00×10^4
ascorbic acid	$^{\bullet}OH$, $^{\bullet}O_2^-$	0.01	30.0
thiourea	$^{\bullet}OH$	0.01	800
NBT	$^{\bullet}O_2^-$	0.01	15.0
DMPO	$^{\bullet}OH$, $^{\bullet}SO_3^-$	0.05% (v/v)	6.50×10^3

[a]Concentrations of $NaHSO_3$ and H_2O_2 were 0.2 and 0.5 mol/L, injection volume was 100 μL, radical scavengers were 50 μL; 7,10-BaPQ was 10 pmol. [b]Average value of three times.

In Table 1, we can find the CL intensity decreased to 30 with the addition of ascorbic acid. As we known, ascorbic acid is an effective active oxygen free radical ($^{\bullet}OH$, $^{\bullet}O_2^-$) scavenger.[32] Therefore, it can be considered that $NaHSO_3$ reacted with H_2O_2 via radical way. $^{\bullet}OH$ radical has been reported in the oxidation of HSO_3^- ion by H_2O_2.[31,33] Thiourea was commonly used as $^{\bullet}OH$ radical scavenger.[33] When thiourea was added into the CL system, strong inhibition of CL intensity by thiourea was observed, which indicated the generations of $^{\bullet}OH$ radical. In addition, the existence of $^{\bullet}OH$ radical can be confirmed by the electron ESR spectrum (Figure 2).

Production of $^{\bullet}SO_3^-$ radical can be identified by inhibition effect of DMPO, which can trap $^{\bullet}SO_3^-$ radical and $^{\bullet}OH$ (Reactions 1 and 2).[34] The CL reaction stopped when the $^{\bullet}SO_3^-$ radical was trapped by DMPO, which lead to the decreasing of CL intensity.

$$DMPO + {}^{\bullet}SO_3^- \rightarrow DMPO/{}^{\bullet}SO_3 \quad (1)$$

$$DMPO + {}^{\bullet}OH \rightarrow DMPO/{}^{\bullet}OH \quad (2)$$

$^{\bullet}SO_3^-$ radical reacted with excess H_2O_2 to give HO_2^- and finally forming $^{\bullet}O_2^-$ radical.[33] NBT is an specific $^{\bullet}O_2^-$ radical scavenger (reaction 3).[35,36] When NBT was added into the $NaHSO_3$-7, 10-BaPQ-H_2O_2 system, CL intensity decreased to 15 (Table 1). Therefore, we can speculate $^{\bullet}O_2^-$ radical was generated in the $NaHSO_3$–7,10-BaPQ–H_2O_2 system, which played a key role in CL emission.

$$NBT^{2+} + {}^{\bullet}O_2^- \rightarrow {}^{\bullet}NBT^+ + O_2 \quad (3)$$

In addition, ESR method was also employed to confirm the existence of $^{\bullet}OH$ and $^{\bullet}SO_3^-$ radicals, which were generated in the $NaHSO_3$–H_2O_2 system. The life times of $^{\bullet}OH$ and $^{\bullet}SO_3^-$ radicals are short, therefore, DMPO was used to trap them.[31,33,34,37] The ESR spectrum of $^{\bullet}OH$ and $^{\bullet}SO_3^-$ radicals is shown in Figure 2A. In this spectrum, $^{\bullet}OH$ and $^{\bullet}SO_3^-$ radicals overlapped.[31,37] Thus, the spectra in 0, 2, and 4 min were compared (Figure 2B). In the $NaHSO_3$–H_2O_2 system, the lifetime of DMPO/$^{\bullet}OH$ is longer than DMPO/$^{\bullet}SO_3^-$, after 4 min, DMPO/$^{\bullet}SO_3^-$ decomposed or reacted with other ions, while DMPO/$^{\bullet}OH$ still existed in the system (Figure 2B).

With the addition of 7,10-BaPQ, a strong distinct approximate 1:3:3:1 four-line spectrum (g = 2.0042) appeared (Figure 2C), which may belong to the semiquinone of 7,10-BaPQ.[38] The irregular peak was unstable, disproportionate in five minutes (Figure 2D).

The construction of 7,10-BaPQ was confirmed by HPLC before and after it reacting with $NaHSO_3$–H_2O_2. The chromatograms showed that 7,10-BaPQ appeared in the same retention time before and after reacting with $NaHSO_3$–H_2O_2 CL system, which means that 7,10-BaPQ returned back to its original structure after CL emission occurred (Figure 3). However, we also found two small peaks appeared in the chromatogram after the reaction, which may be generated by the reaction of semiquinone with other radicals or ions in the $NaHSO_3$–H_2O_2 system.

The cut off filters (400–640 nm) were used to determine the CL emission spectrum of $NaHSO_3$–H_2O_2. The CL emission from $NaHSO_3$–H_2O_2 was too weak to measure the CL wavelength. Sodium dodecyl sulfate, which is a common surfactant, was applied to enhance the CL intensity. As shown in Figure 4a, a wide peak with a maximum appeared in the spectrum of $NaHSO_3$–H_2O_2 system, which may be ascribed to excited sulfur dioxide. The maximum of the peak moved to 440 nm after addition of 7,10-BaPQ (Figure 4b).

CL Mechanism. On the basis of the study of radicals, products, and CL emission spectrum in the $NaHSO_3$–7,10-BaPQ–H_2O_2 system, mechanism of this CL system can be speculated as the following reactions and graphically showed in Scheme 1.

First, HSO_3^- reacted with H_2O_2 via nucleophilic dispalcement to form a peroxomonosulfurous acid intermediate,[29,30] which decomposed to generate $^{\bullet}OH$ and $^{\bullet}SO_3^-$ radicals (reaction 4).[31,33,37]The $^{\bullet}OH$ radical as a strong oxidant reacted with HSO_3^- to give $^{\bullet}SO_3^-$ radical in a rapid rate.[39,40]

$$H_2O_2 + HSO_3^- \rightleftharpoons \text{[peroxomonosulfurous acid intermediate]} \rightarrow {}^{\bullet}OH + {}^{\bullet}SO_3^- \quad (4)$$

$$^{\bullet}OH + HSO_3^- \rightarrow {}^{\bullet}SO_3^- + H_2O \quad (5)$$

dx.doi.org/10.1021/ac2032063 | Anal. Chem. 2012, 84, 3215–3221

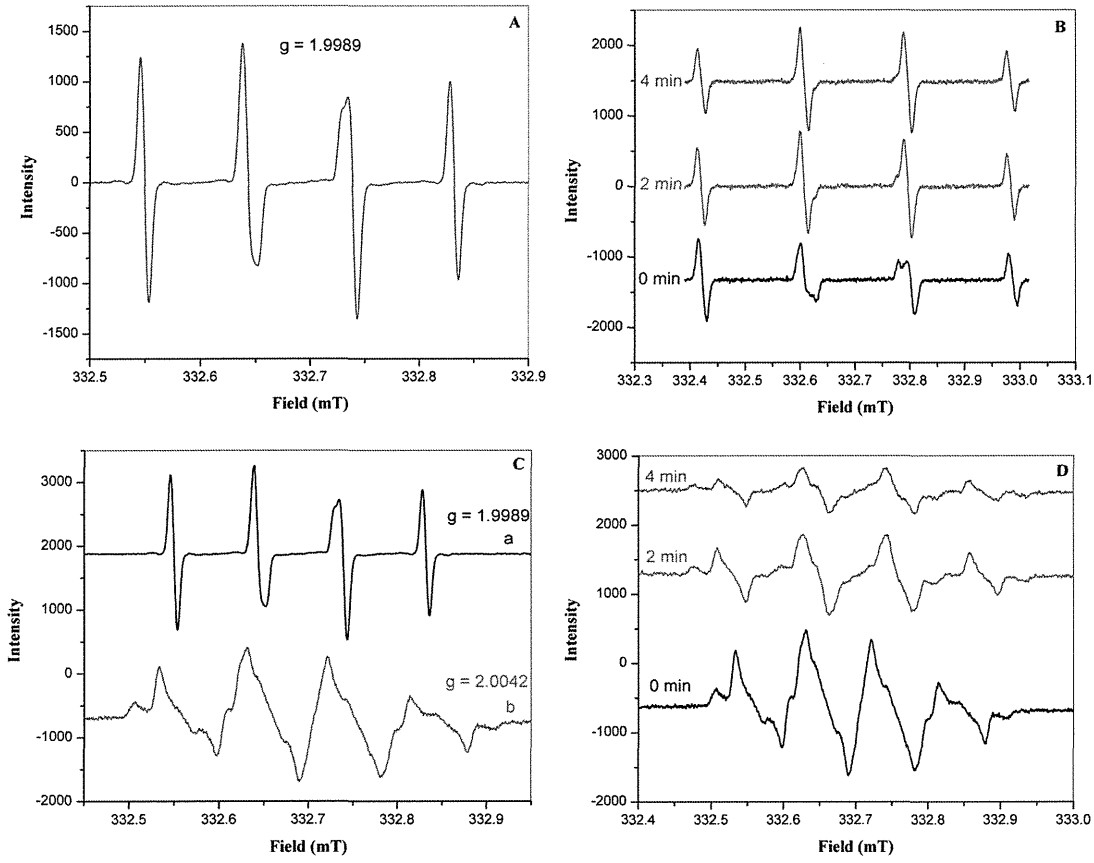

Figure 2. ESR spectra (A) $^{\bullet}OH$ and $^{\bullet}SO_3^-$ radical in $NaHSO_3$–H_2O_2 CL system. (B) DMPO/$^{\bullet}OH$ and DMPO/$^{\bullet}SO_3^-$ in 0, 2, 4 min. (C) ESR spectra of $NaHSO_3$–H_2O_2 CL system before (a) and after addition of 7,10-BaPQ (b). (D) ESR spectra of semiquinone radicals from 7,10-BaPQ. Conditions: DMPO 0.2 mol/L prepared in water; $NaHSO_3$ 0.1 mol/L, H_2O_2 0.5 mol/L. Each volume of DMPO, $NaHSO_3$, and H_2O_2 was 30 μL.

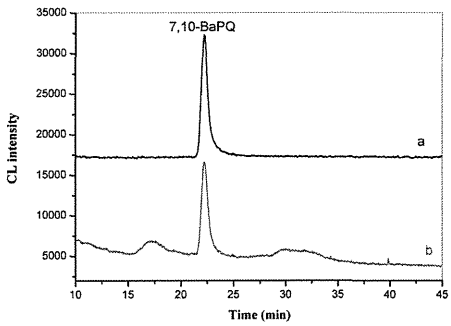

Figure 3. Chromatograms of 7,10-BaPQ (1.5 pmol/injection) before (a) and after (b) reacting with $NaHSO_3$–H_2O_2 system.

$^{\bullet}SO_3^-$ radical reacted with H_2O_2 to give $^{\bullet}O_2^-$ radical (reactions 6 and 7),[33] which is an important radical in the CL system.

$$^{\bullet}SO_3^- + H_2O_2 \rightarrow HSO_3^- + HO_2^{\bullet} \quad (6)$$

$$HO_2^{\bullet} \rightarrow H^+ + {}^{\bullet}O_2^- \quad (7)$$

Several groups have reported the reduction of quinone to semiquinone by $^{\bullet}O_2^-$ radical.[41–44] CL emission was observed with the decay of excited semiquinone,[45–47] which was then oxidized to 7,10-BaPQ (reaction 8).

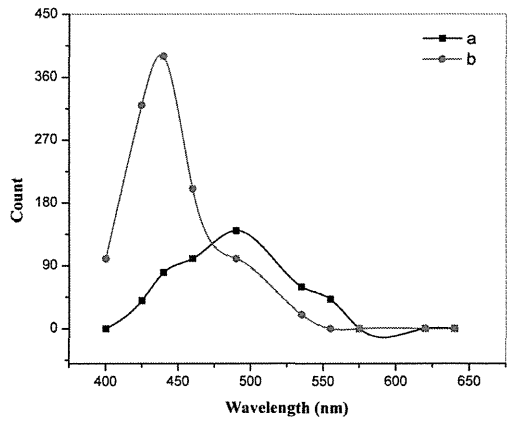

Figure 4. CL emission spectrum of $NaHSO_3$-7, 10-BaPQ-H_2O_2 CL system. (a) Emission spectrum of $NaHSO_3$–H_2O_2 system. (b) Emission spectrum of $NaHSO_3$–7,10-BaPQ–H_2O_2 system.

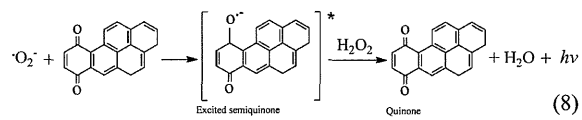

(8)

Other PAH quinones (1,4-benzoquinone, 1,4-naphthoquinone, 1,4-anthraquinone, and 1,4-chrysenequinone), whose

Scheme 1. Mechanism of $NaHSO_3$–7,10-BaPQ–H_2O_2 CL System

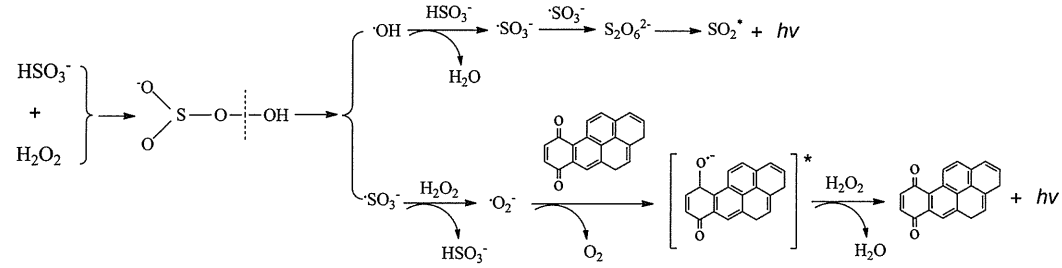

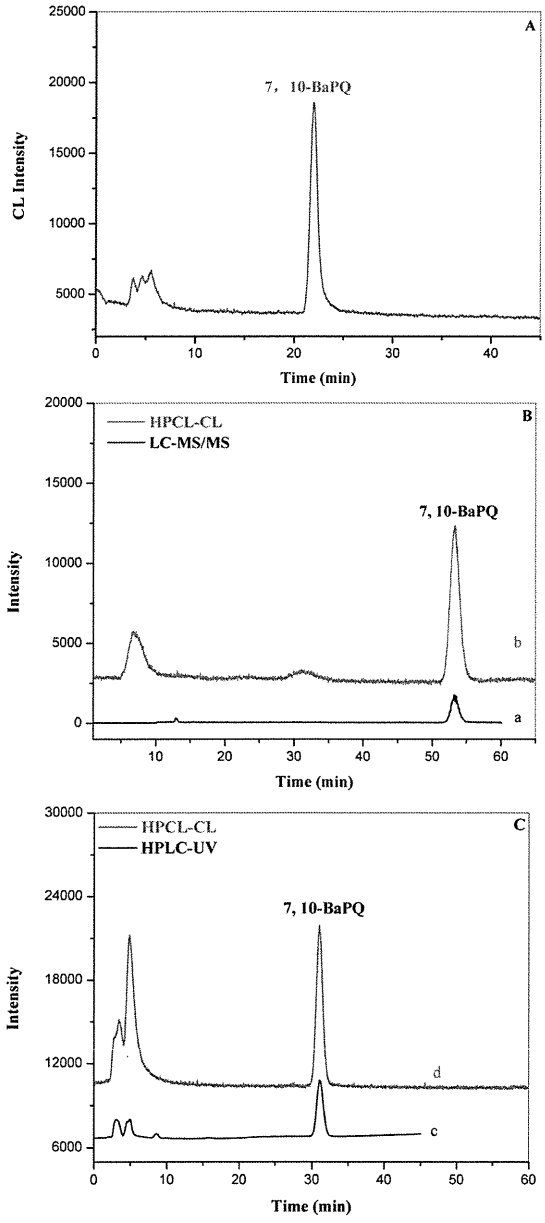

Figure 5. (A) Typical chromatogram of standard 7,10-BaPQ (1.5 pmol per injection) in HPLC-$NaHSO_3$–H_2O_2 system. (B) Chromatograms of 7,10-BaPQ in HPLC-CL (7,10-BaPQ, 1.0×10^{-8} mol/L) and in HPLC-UV (7,10-BaPQ, 1.0×10^{-6} mol/L). (C) Chromatograms of 7,10-BaPQ in HPLC-CL and in LC-MS/MS (7,10-BaPQ, 1.0×10^{-7} mol/L).

structures are similar to 7,10-BaPQ, were also added into the $NaHSO_3$–H_2O_2 system. It was found that with the increase of benzene ring, the CL intensity increased. However, the CL intensities of the PAH quinones were still much lower than 7,10-BaPQ.

Furthermore, generation of excited sulfur dioxide (SO_2*) from $NaHSO_3$–H_2O_2 reaction has been reported.[33] $^{\bullet}SO_3^-$ radical dimerized to give $S_2O_6^{2-}$ ion (reaction 9). SO_2* was produced by the decomposition of $S_2O_6^{2-}$ ion (reaction 10).[48,49]

$$^{\bullet}SO_3^- + {}^{\bullet}SO_3^- \rightarrow S_2O_6^{2-} \quad (9)$$

$$S_2O_6^{2-} \rightarrow SO_4^{2-} + SO_2^* \quad (10)$$

Analytical Figures of Merit. The CL system was developed as an ultrahighly sensitive postcolumn detection for the determination of 7,10-BaPQ in airborne particulates. Organic solvents which were used for HPLC mobile phase have critical effect on $NaHSO_3$–7,10-BaPQ–H_2O_2 CL system. Methanol and acetonitrile were compared. It was found 80% (v/v) methanol/water gave baseline separation of 7,10-BaPQ from interference compounds and highest peak height. The typical chromatogram of standard 7,10-BaPQ in the optimized conditions is shown in Figure 5A.

The proposed method was evaluated in terms of linearity, sensitivity, and precision. Calibration curve was obtained by the standard 7,10-BaPQ solution over the range from 50 fmol to 20 pmol per injection. A highly linear relationship between peak height and concentrations was obtained (12 calibration points; $R^2 = 0.9995$). The slope and intercept of the regression equation of calibration curve were 1.22×10^{12} and −463. The detection limit ($S/N = 3$) of 7,10-BaPQ was 30 fmol per injection. Till now, LC-MS/MS is the most sensitive method for the determination of 7,10-BaPQ.[50] However, the sensitivity of the proposed HPLC-CL method for detecting 7,10-BaPQ was 2 orders of magnitude higher than LC-MS-MS method and 3 orders of magnitude higher than HPLC-UV (Figure 5B and Figure 5 C). The precision and accuracy of the proposed method for determination of 7,10-BaPQ were investigated with

Table 2. Precision of the Method for Determining 7,10-BaPQ in Airborne Particulates and Recovery of 7,10-BaPQ in Airborne Particulates

	intraday (n = 3)			interday (n = 3)		
added (pmol)	0	15.0	50.0	0	15.0	50.0
found (pmol)	3.90	19.3	53.7	3.90	18.5	54.1
recovery (%)[a]		102.7	99.6		97.3	100.4
RSD (%)	7.80	4.80	4.80	5.70	1.60	1.00

[a]Expressed as (found amount − nonspiked amount)/added amount.

dx.doi.org/10.1021/ac2032063 | Anal. Chem. 2012, 84, 3215–3221

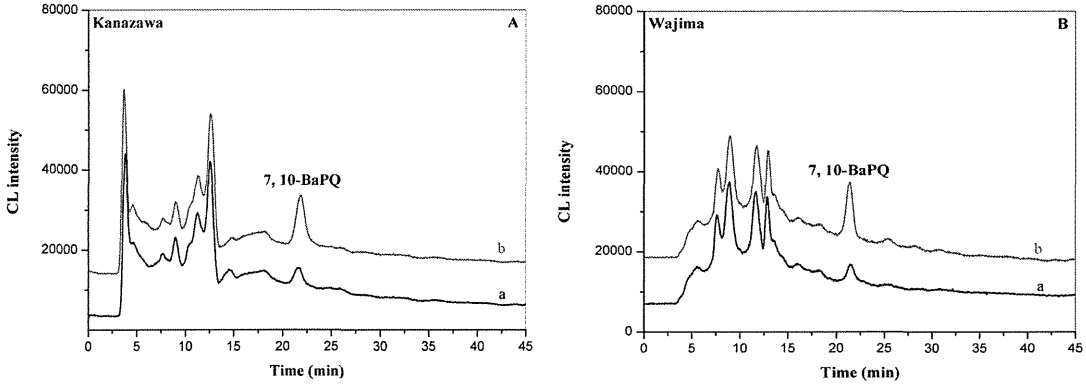

Figure 6. Chromatograms of 7,10-BaPQ (a) in airborne particulates and (b) airborne particulates spiked with 1.5 pmol 7,10-BaPQ.

spiking the airborne particulates at two different level of 7,10-BaPQ standard solutions. The results are shown in Table 2.

Determination of 7,10-BaPQ in Airborne Particulates. Benzene[*a*]pyrene (BaP), which is one of most important PAH pollutants in environment, has high carcinogenicity, mutagenicity. In airborne particulates, BaP reacted with some reactive oxygen species to generate BaP quinones. The toxicity of these BaPQs is higher than BaP. Therefore, it is urgency to monitoring the concentration of these BaPQs. However, common methods, such as LC-MS/MS, GC-MS/MS, HPLC-UV, and HPLC-fluorescence, are difficult to detect the BaPQs because their sensitivities are not high enough for the really application, especially for 7,10-BaPQ.[50] The proposed HPLC-CL method was employed to determine 7,10-BaPQ in airborne particulates successfully. Average concentrations of 7,10-BaPQ in Kanazawa, Japan in December 2010 and Wajima, Japan in October 2007 were 2.0 and 1.6 pg/m^3, respectively. Chromatograms of airborne particulates were show in Figure 6A and B.

CONCLUSIONS

7,10-BaPQ (10 pmol) is found to greatly enhance the ultra-weak CL emission, which emits from $NaHSO_3$–H_2O_2 system. The radicals of $NaHSO_3$–7,10-BaPQ–H_2O_2 system are confirmed by CL spectrum, radical scavengers and ESR spectrum. Superoxide ($^{\bullet}O_2^-$) radical reacted with 7,10-BaPQ to give semiquinone which give out a strong CL signal at 440 nm. An ultrasensitive CL detection method was established based on this mechanism.

AUTHOR INFORMATION

Corresponding Author

*Phone: +86-10-62792343 (J.-M.L.); +81-76-2344458 (K.H.). Fax: +86-10-62792343 (J.-M.L.); +81-76-2344456 (K.H.). E-mail: jmlin@mail.tsinghua.edu.cn (J.-M.L.); hayakawa@mail.p.kanazawa-u.ac.jp (K.H.).

Notes

The authors declare no competing financial interest.

ACKNOWLEDGMENTS

This work was supported by National Natural Science Foundation of China (Nos. 20935002, 90813015).

REFERENCES

(1) Yang, Y.; Vanmetre, P. C.; Mahler, B. J.; Wilson, J. T.; Ligouis, B.; Muhitrazzaque, M.; Schaeffer, D. J.; Werth, C. J. J. *Environ. Sci. Technol.* **2010**, *44*, 1217–1223.

(2) Castro, D.; Slezakova, K.; Delerue-Matos, C.; Alvim-Ferraz, M.; Morais, S.; Pereira, M. *Atmos. Environ.* **2011**, *45*, 1799–1808.

(3) Marr, L. C.; Grogan, L. A.; WÖhrnschimmel, H. Y.; Molina, L. T.; Molina, M. J. *Environ. Sci. Technol.* **2004**, *38*, 2584–2592.

(4) Wang, J.; Levendis, Y. A.; Richter, H.; Howard, J. B.; Carlson, J. *Environ. Sci. Technol.* **2001**, *35*, 3541–3552.

(5) Kishikawa, N.; Morita, S.; Wada, M.; Ohba, Y.; Nakashima, K.; Kuroda, N. *Anal. Sci.* **2004**, *20*, 129–132.

(6) Kameda, T.; Akiyama, A.; Toriba, A.; Tang, N.; Hayakawa, K. *Environ. Sci. Technol.* **2011**, *45*, 3325–3332.

(7) Kojima, Y.; Inazu, K.; Hisamatsu, Y.; Okochi, H.; Baba, T. *Atmos. Environ.* **2010**, *44*, 2873–2880.

(8) Walgraeve, C.; Demeestere, K.; Dewulf, J.; Zimmermann, R.; Langenhove, H. V. *Atmos. Environ.* **2010**, *44*, 1831–1846.

(9) Zhao, Y.; Xia, Q; Yin, J. J.; Yu, H.; Fu, P. *Chemosphere* **2011**, *85*, 83–91.

(10) Motoyama, Y.; Bekki, K.; Chung, S.; Tang, N.; Kameda, T.; Toriba, A.; Taguchi, K.; Hayakawa, K. *J. Health Sci.* **2009**, *55*, 845–850.

(11) Bolton, J. L.; Thacher, G. R. J. *Chem. Res. Toxicol.* **2008**, *21*, 93–101.

(12) Ma, B.; Carr, B. A.; Krolikowski, P.; Chang, F. *Chem. Res. Toxicol.* **2007**, *20*, 72–78.

(13) Terashima, I.; Suzuki, N.; Shibutani, S. *Biochemistry* **2001**, *40*, 166–172.

(14) Kumagai, Y.; Nakajima, H.; Midorikawa, K.; Homma-Takeda, S.; Shimojo, N. *Chem. Res. Toxicol.* **1998**, *11*, 608–613.

(15) Taguchi, K.; Kumagai, Y.; Endo, A.; Kikushima, M.; Ishii, Y.; Shimojo, N. *J. Health Sci.* **2001**, *47*, 571–574.

(16) Hayakawa, K.; Bekki, K.; Yoshita, M.; Tachikawa, C.; Kameda, T.; Tang, N.; Toriba, A.; Hosoi, S. *J. Health Sci.* **2011**, *57*, 274–280.

(17) Cho, A. K.; Stefano, E. D.; You, Y.; Rodriguez, C. E.; Schmitz, D. A.; Kumagai, Y.; Miguel, A.; Eiguren-Fernandez, A.; Kobayashi, T.; Avol, E.; Froines, J. R. *Aerosol Sci. Technol.* **2004**, *38*, 68.

(18) Koeber, R.; Bayona, J. M.; Niessner, R. *Environ. Sci. Technol.* **1999**, *33*, 1552–1558.

(19) Lintelmann, J.; Fischer, K.; Matuschek, G. *J. Chromatogr. A* **2006**, *1133*, 241–247.

(20) Delhomme, O.; Millet, M.; Herckes, P. *Talanta* **2008**, *74*, 703–710.

(21) Lintelmann, J.; Fischer, K.; Karg, E.; Schroppel, A. *Anal. Bioanal. Chem.* **2005**, *385*, 508–519.

(22) Kishikwa, N.; Nakao, M.; Elgawish, M.; Ohyama, K.; Nakashima, K.; Kuroda, N. *Talanta* **2011**, *85*, 809–812.

(23) Kishikawa, N.; Nakashima, H.; Ohyama, K.; Nakashima, K.; Kuroda, N. *Talanta* **2010**, *81*, 1852–1855.

(24) Kishikawa, N.; Wada, M.; Ohba, Y.; Nakashima, K.; Kuroda, N. *J. Chromatogr. A* **2004**, *1057*, 83–88.

(25) Kameda, T.; Goto, T.; Toriba, A.; Tang, N.; Hayakawa, K. *J. Chromatogr. A* **2009**, *1216*, 6758–6761.

(26) Ahmed, S.; Kishikawa, N.; Ohyama, K.; Maki, T.; Kurosaki, H.; Nakashima, K.; Kuroda, N. *J. Chromatogr. A* **2009**, *1216*, 3977−3984.
(27) Ahmed, S.; Fujii, S.; Kishikawa, N.; Ohba, Y.; Nakashima, K.; Kuroda, N. *J. Chromatogr. A* **2006**, *1133*, 76−82.
(28) Li, R.; Kameda, T.; Li, Y.; Toriba, A.; Tang, N.; Hayakawa, K.; Lin, J.-M. *Talanta* **2011**, *85*, 2711−2714.
(29) Hoffmann, M. R.; Edwards, J. O. *J. Phys. Chem.* **1975**, *79*, 2096−2098.
(30) Mcardle, J. V.; Hoffmann, M. R. *J. Phys. Chem.* **1983**, *87*, 5425−5429.
(31) Shi, X. *J. Inorg. Biochem.* **1994**, *56*, 155−165.
(32) Liang, S.; Zhao, L.; Zhao, B.; Zhang, B.; Lin, J. -M. *J. Phys. Chem. A* **2008**, *112*, 618−623.
(33) Xue, W.; Lin, Z.; Chen, H.; Lu, C.; Lin, J.-M. *J. Phys. Chem. C* **2011**, *115*, 21707−21714.
(34) Mottey, C.; Mason, R. *Arch. Biochem. Biophys.* **1988**, *267*, 681−689.
(35) Lin, J.-M.; Yamada, M. *Anal. Chem.* **1999**, *71*, 1760−1766.
(36) Bielski, B. H. J.; Shiue, G. G.; Bajuk, S. *J. Phys. Chem.* **1980**, *84*, 830−833.
(37) Ozawa, T.; Hanaki, A. *Biochem. Biophys. Res. Commun.* **1987**, *142*, 410−416.
(38) Song, Y.; Buettner, G. R.; Parkin, S.; Wagner, B. A.; Robertson, L. W.; Lehmer, H. J. *J. Org. Chem.* **2008**, *73*, 8296−8304.
(39) Huie, R. E.; Neta, P. *Atmos. Environ.* **1987**, *21*, 1743−1747.
(40) Neta, P.; Huie, R. E. *J. Phys. Chem. Ref. Data* **1988**, *17*, 1027−1284.
(41) Bielski, B. H. J.; Cabelii, D. E.; Arudi, R. E. *J. Phys. Chem. Ref. Data.* **1985**, *14*, 1041−1100.
(42) Garg, S.; Rose, A. L.; Waite, T. *Photochem. Photobiol.* **2007**, *83*, 904−913.
(43) Samoilova, R. I.; Crofts, A. R.; Dikanov, S. A. *J. Phys. Chem. A* **2011**, *115*, 11589−11593.
(44) Kawashima, T.; Ohkubo, K.; Fukuzmi, S. *Phys. Chem. Chem. Phys.* **2011**, *13*, 3344−3352.
(45) Stauff, J.; Bartolmes, P. *Angew. Chem., Int. Ed. Engl.* **1970**, *9*, 307−308.
(46) Slawinska, D. *Photochem. Photobiol.* **1978**, *28*, 453−458.
(47) Chen, X.; Zhao, L.; Wang, X.; Lin, J.-M. *Anal. Sci.* **2007**, *23*, 1189−1193.
(48) Kato, M.; Yamada, M.; Suzuki, S. *Anal. Chem.* **1984**, *56*, 2529−2534.
(49) Yu, X.; Bao, J. *J. Lumin.* **2009**, *129*, 973−978.
(50) Koeber, R.; Nissner, R.; Bayona, J. *Fresenius' J. Anal. Chem.* **1997**, *359*, 267−273.

Journal of Chromatography B, 893–894 (2012) 173–176

Contents lists available at SciVerse ScienceDirect

Journal of Chromatography B

journal homepage: www.elsevier.com/locate/chromb

Short communication

Analysis of 8-hydroxy-2′-deoxyguanosine in human urine using hydrophilic interaction chromatography with tandem mass spectrometry

Chiemi Hosozumi[a], Akira Toriba[a,*], Thanyarat Chuesaard[a], Takayuki Kameda[a], Ning Tang[b], Kazuichi Hayakawa[a]

[a] Institute of Medical, Pharmaceutical and Health Sciences, Kanazawa University, Kakuma-machi, Kanazawa 920-1192, Japan
[b] Department of Public Health, Hyogo College of Medicine, 1-1 Mukogawa-cho, Nishinomiya 663-8501, Japan

ARTICLE INFO

Article history:
Received 10 July 2011
Accepted 26 February 2012
Available online 3 March 2012

Keywords:
Hydrophilic interaction chromatography
Tandem mass spectrometry
8-Hydroxy-2′-deoxyguanosine
Urine
Oxidative stress

ABSTRACT

Urinary 8-hydroxy-2′-deoxyguanosine (8-OHdG) is a widely used noninvasive biomarker of oxidative stress. A selective, sensitive and rapid method for determining 8-OHdG in human urine was developed using hydrophilic interaction chromatography–tandem mass spectrometry (HILIC–MS/MS) with electrospray ionization. 8-OHdG and isotopically labeled 8-OHdG (internal standard) were separated on a HILIC column with a mobile phase of 10 mM ammonium acetate: acetonitrile (1:9, v/v) within 10 min and detected by using a positive electrospray ionization interface under the selected reaction monitoring mode. The detection limits of 8-OHdG (corresponding to a signal-to-noise ratio of 3) for the HILIC-MS/MS system and the conventional method using a reversed-phase column with MS/MS were 1.0 and 26.0 fmol/injection, respectively. The proposed method makes it possible to monitor the basal level of urinary 8-OHdG from non-exposed healthy subjects and can be used for large-scale human studies.

1. Introduction

Oxidative stress in an organism arises from excessive generation of reactive oxygen species (ROS) such as superoxide radicals, hydrogen peroxide and hydroxyl radicals or from depletion of antioxidants [1]. The production of ROS can be induced by both endogenous and exogenous factors [2]. While endogenous factors include physiological processes, exogenous factors include environmental sources such as smoking, diet and pollution [3]. ROS may cause oxidative damage to nucleic acids, proteins, and lipids [2]. In particular, oxidative damage to DNA has been associated with numerous pathological conditions, having both genetic and epigenetic consequences [4–6]. To understand how ROS affect normal and pathological processes, an indicator to assess oxidative stress *in vivo* is required.

The oxidized product of DNA, 8-hydroxy-2′-deoxyguanosine (8-OHdG), is the most frequently measured biomarker of the oxidative stress [7,8]. The 8-OHdG has been analyzed in various kinds of samples, such as urine, serum, peripheral blood leukocyte, and organ tissue [9]. Measurements of 8-OHdG in urine samples are especially well-suited to large-scale human studies and clinical applications because they are noninvasive [10,11]. Urinary 8-OHdG has been analyzed by several methods, such as enzyme-linked immunosorbent assay (ELISA) [12,13], high-performance liquid chromatography with electrochemical detection (HPLC-ECD) [14], gas chromatography with mass spectrometry (GC/MS) [15,16], and liquid chromatography with tandem mass spectrometry (LC/MS/MS) [17–26]. The ELISA method suffers from the problem of non-selectivity because the antibody may cross-react with other substances present in urine [12,27,28]. HPLC-ECD has often been used [29], but it suffers from possible interference from the biological matrix, incompatibility of a stable isotope labeled internal standard [16,21]. For GC/MS analysis, 8-OHdG must be purified by HPLC and derivatized before analysis [15,16,28].

LC–MS/MS has been increasingly applied to detect urinary 8-OHdG. LC–MS/MS, when combined with the isotope dilution technique, is highly selective, sensitive, and accurate, and does not require derivatization [28]. In most of previous LC–MS/MS studies, reversed-phase columns have been used to separate 8-OHdG [17–26]. As a polar compound, 8-OHdG is hardly retained on a reversed-phase column, even though aqueous mobile phases are used. Such poor retention of 8-OHdG and its insufficient separation from polar components in the matrix may lead to matrix effects, which can increase or decrease the 8-OHdG MS signal [30]. In addition, aqueous mobile phases that are used to retain polar compounds on reversed-phase columns are not suited for electrospray ionization (ESI) conditions [30]. Indeed, urinary 8-OHdG levels have even been below the detection limit of LC–MS/MS

* Corresponding author. Tel.: +81 76 234 4457; fax: +81 76 234 4456.
E-mail address: toriba@p.kanazawa-u.ac.jp (A. Toriba).

1570-0232/$ – see front matter © 2012 Elsevier B.V. All rights reserved.
doi:10.1016/j.jchromb.2012.02.043

method (7.5 fmol/injection, $S/N = 3$) [27,31]. Therefore, a more sensitive LC–MS/MS method is required to measure basal levels of urinary 8-OHdG in non-exposed healthy subjects.

In recent years, hydrophilic interaction chromatography (HILIC) has been increasingly used in LC–MS/MS for analyzing polar compounds such as metabolites in biological samples. Under HILIC conditions, the analyte interacts with a hydrophilic stationary phase and is eluted with a high concentration of organic solvent (typically acetonitrile with a small percentage of water/buffer). The highly organic mobile phase can result in increased sensitivity with ESI-MS detection [30,32].

In this study, we developed an improved LC–MS/MS method for measuring urinary 8-OHdG using a HILIC column. We found that the HILIC column provided much greater sensitivity than a conventional reversed-phase column with the same MS/MS detection conditions.

2. Experimental

2.1. Materials

The 8-OHdG and [$^{15}N_5$]8-OHdG were purchased from Sigma (MO, USA) and Cambridge Isotope Laboratories (MA, USA), respectively. HPLC grade acetonitrile was obtained from Kanto Chemical (Tokyo, Japan), and water from a Milli-Q water purification system (Millipore, Bedford, MA, USA). All other chemicals and solvents used were of an analytical grade.

2.2. Sample preparation

Urinary samples were pretreated as described previously with a slight modification [22,28]. After centrifugation at 2150 × *g* for 10 min, a 100 μL aliquot of each supernatant was diluted with 900 μL of water and spiked with 10 pmol of the stable isotope labeled internal standard (IS), [$^{15}N_5$]8-OHdG. The diluted sample was subjected to solid-phase extraction using Oasis HLB cartridge (3 cc, 60 mg; Waters, Milford, MA, USA) that had been primed with 1 mL of methanol and 1 mL of water. After sample loading, the cartridge was sequentially washed with 1 mL of water. The 8-OHdG was eluted from the cartridge with 500 μL of water: acetonitrile (1:1, v/v), and evaporated to dryness using a centrifugal vacuum evaporator. The residue was redissolved in 100 μL of water: acetonitrile (1:9, v/v), and an aliquot of 20 μL was injected into the LC–MS/MS system.

2.3. 8-OHdG analysis by HILIC-MS/MS

2.3.1. Apparatus and chromatographic conditions

The Agilent 1100 series LC system consists of a G1379A degasser, a G1312A binary pump, a G1367A autosampler, and a G1316A column oven (all from Agilent Technologies, Palo Alto, CA, USA). The chromatographic separation of 8-OHdG in the pretreated urine samples was performed on a COSMOSIL HILIC (150 mm × 2.0 mm i.d., 5 μm, Nacalai Tesque, Kyoto, Japan), kept at the temperature of 40 °C. The column was eluted isocratically with 10 mM ammonium acetate: acetonitrile (1:9, v/v) at a flow rate of 0.4 mL/min. The retention time of the analyte was optimized by varying the mobile phase acetonitrile content between 70% and 95% with 10 mM ammonium acetate and by varying the aqueous buffer concentration between 10 and 50 mM with 90% acetonitrile. The retention factor (k) of 8-OHdG was defined as $k = (t_R - t_0)/t_0$, where t_R and t_0 are the retention times of the analyte and the hold-up time, respectively. Sample volumes of 20 μL were injected for each analysis. The mass spectrometric analyses were performed using an API 4000 Q-Trap tandem mass spectrometer (Applied Biosystems, CA, USA) equipped with an electrospray ionization (ESI) and operated in a positive ion mode. Sensitivity of the selective reaction monitoring (SRM) was optimized by testing with an infusion of 8-OHdG under the mobile phase condition. The mass spectrometer was operated under SRM mode of the transitions at m/z 284.3 → 167.9 for 8-OHdG and at m/z 289.1 → 173.0 for [$^{15}N_5$]8-OHdG (IS) with dwell times of 1000 ms. The spray voltage was maintained at 5.5 kV. Nitrogen gas was used as the collision gas (4 psi) and curtain gas (20 psi), whereas zero grade air was used as the nebulizer gas (40 psi) and heated gas (60 psi). Source temperature was set at 600 °C. The collision energy and declustering potential were set at 19 V and 71 V, respectively. Analyst software (version 1.4, Applied Biosystems) was used to control the LC–MS/MS system, and to acquire and process the data.

2.3.2. Calibration curve and validation

Calibration curves for quality control (QC) samples were obtained from the ratio of peak areas of 8-OHdG and [$^{15}N_5$]8-OHdG (IS) using 0.1 mL human urine samples from six humans spiked with 8-OHdG at final concentrations of 0.2, 5, 10, 30, 50, 100 nmol/L. Standard curves were also obtained from plotting the peak area ratio against the same six concentrations of the analyte as the spiked urine samples ($n = 6$ for each). The lower limit of quantification (LLOQ) was determined as the lowest standard on the calibration curve that gave a signal-to-noise ratio of more than ten and reached a precision of 20% and an accuracy of 80–120%. The limit of detection (LOD) was determined as the lowest concentration that gave a signal-to-noise ratio of more than three. To evaluate the intra and inter-day accuracy and precision, the stock solution of 8-OHdG was added to urine at concentrations of 10 and 50 nmol/L in 0.1 mL urine. The spiked samples, together with non-spiked samples, were analyzed using HILIC–MS/MS and 8-OHdG concentrations were calculated using a standard curve. Accuracy was expressed as the ratio of the quantified concentration to the known concentration of 8-OHdG. To evaluate the intra-day precision, the non-spiked samples and the samples spiked at the two levels were prepared five times per day. The inter-day precision was determined using five independent experiments. The precision was calculated as the relative standard deviation (RSD) (%) of the replicates.

2.4. 8-OHdG analysis by LC–MS/MS using reversed-phase column

On the basis of previously reported LC–MS/MS method [25], chromatographic separation of 8-OHdG and [$^{15}N_5$]8-OHdG (IS) in urine samples was performed on a XBridge C_{18} column (150 mm × 2.1 mm i.d., 3.5 μm, Waters) with a guard column (XBridge C_{18} column, 10 mm × 10 mm i.d., 5 μm, Waters). The elution was run isocratically with a mobile phase consisting of 10 mM ammonium acetate: methanol (19:1, v/v) at a flow rate of 0.4 mL/min. The column temperature was set at 40 °C. The mass spectrometric detection was carried out by the same SRM transitions as the HILIC mode.

3. Results and discussion

3.1. Mass spectrometry and chromatography

The full scan mass spectrum of 8-OHdG in the positive ESI mode and the fragmentation pattern of protonated molecular ion $[M+H]^+$ observed in this study were consistent with those of previous studies [17,18,24,26]. The transition from the molecular ion $[M+H]^+$ to the most intense fragment was recorded in the selective reaction monitoring (SRM) acquisition mode. The main product ions of 8-OHdG and [$^{15}N_5$]8-OHdG (IS) were m/z 167.9 and 173.0 $[M+H-116]^+$, respectively. Therefore, the $[M+H]^+ \rightarrow [M+H-116]^+$ transition was used in the SRM mode.

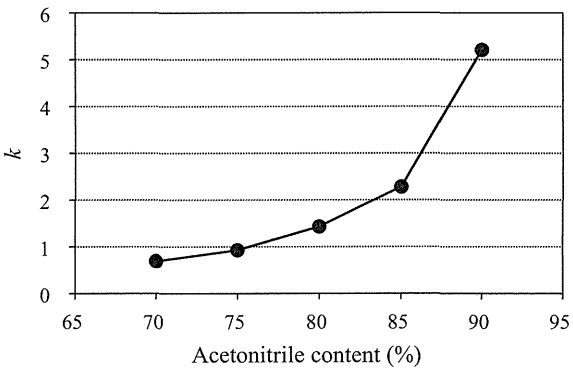

Fig. 1. Effect of acetonitrile content in the mobile phase on the retention of 8-OHdG.

We examined the effect of the acetonitrile concentration in the mobile phase of the HILIC column on the retention time of the analytes. The column was operated under isocratic elution conditions using acetonitrile concentration between 70 and 95%, at the interval of 5%. The retention factor (k) increased with the increasing acetonitrile concentration (Fig. 1). The high content of acetonitrile increases the hydrophilic interactions between the analytes and the stationary phase [33]. At 95% acetonitrile, 8-OHdG was retained for over 15 min on the column and its peak shape was broad. The retention time of charged analytes can be affected by adding salt to the mobile phase due to the electrostatic interactions between the column and analytes [33,34]. For a salt, we selected ammonium acetate because of its solubility in concentrated acetonitrile solutions, and its volatility at the ion source. The effect of the buffer concentration in the mobile phase on the retention of the analyte was investigated in the range 10–50 mM. Increasing the buffer concentration only slightly decreased the retention and did not influence the peak shape (data not shown). Finally, the analytes were separated by isocratic elution with 10 mM ammonium acetate: acetonitrile (1:9, v/v). The analyte and the internal standard eluted within 10 min using the optimized mobile phase (Fig. 2, A-1 and A-2).

3.2. Calibration curve and validation

The calibration curve for the standard compound was linear ($r^2 > 0.999$) for concentrations in the range of 0.2–100 nmol/L (LLOQ: 0.2 nmol/L), which covers the lower range of the reported levels of 8-OHdG in human urine [29], and the slope was 0.00630 ± 0.00026 (mean ± S.D. RSD, 4.1%).

Representative SRM chromatograms for the analyte and the internal standard of a urine sample from a non-smoker showed that the physiological components of the urine did not interfere with the identification and quantification of the analytes in the chromatograms (Fig. 2, B-1 and B-2). The matrix effect on the mass spectrometric response was evaluated by comparing the slope of the calibration curve with the slope obtained in the presence of urine matrix. Six curves were obtained using six different urine samples, each spiked with six different amounts of 8-OHdG. The mean slope was 0.00655 ± 0.00043 (mean ± S.D., RSD, 6.6%), which was almost identical to the mean slope obtained with the standard solutions. This clearly showed that the matrix did not affect the calibration curve. Therefore, 8-OHdG was quantified by using the calibration curve obtained from the standard solution.

The precision and accuracy of 8-OHdG determination in human urine with the HILIC–MS/MS system were examined by adding two different known amounts of 8-OHdG to a urine sample. The RSDs of the intra-day precision assay ($n = 5$) were in the range 2.3–2.6%, and those of the inter-day assay ($n = 5$) were in the range 2.1–4.0% (Table 1). The accuracy values (%) of the intra-day study and the inter-day assay were in the range 96–102%. Both intra and inter-day precision and accuracy values were satisfactory for determining 8-OHdG in human urine.

3.3. Comparison of the HILIC column with a reversed-phase column

The instrumental detection limit of 8-OHdG measured by the HILIC–MS/MS was 1.0 fmol/injection (signal-to-noise ratio, $S/N > 3$). In contrast, the detection limit achieved with a reversed-phase column and the same detection system was 26.0 fmol/injection under optimal instrumental conditions. Our detection limit of 1.0 fmol

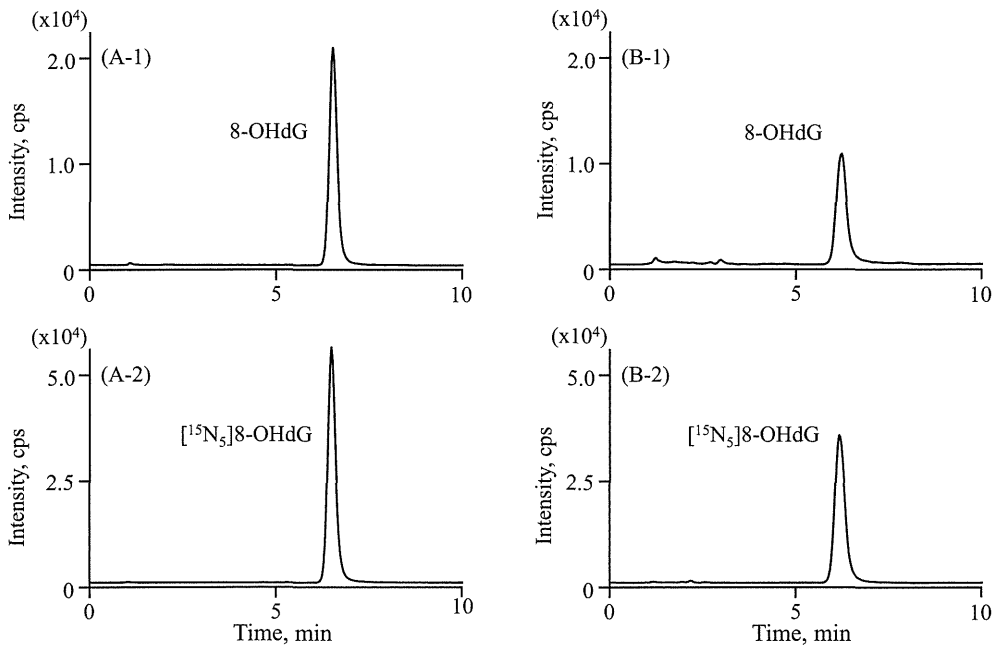

Fig. 2. Representative SRM chromatograms (transition: m/z 284.3 → 167.9 for 8-OHdG and m/z 289.1 → 173.0 for the internal standard ([$^{15}N_5$]8-OHdG)) of a standard solution corresponding to 200 fmol 8-OHdG/injection (A) and a non-smoker urine sample (B) (A-1 and B-1 panels for 8-OHdG; A-2 and B-2 panels for the internal standard).

Table 1
Precision and accuracy in the determination of 8-OHdG in urine samples.

	Intra-day assay ($n=5$)			Inter-day assay ($n=5$)		
Added amounts (pmol/mL urine)	0	10	50	0	10	50
Found ± SD (pmol/mL urine)	17.5 ± 0.4	27.0 ± 0.7	68.5 ± 1.6	16.8 ± 0.4	26.9 ± 0.7	67.5 ± 2.7
RSD (%)	2.3	2.6	2.4	2.1	2.8	4.0
Accuracy (%)	–	96	102	–	101	101

was considerably lower than the detection limits reported for other previous LC–MS/MS methods: 20 fmol [17], 7 fmol ($S/N=3$) [18], 5 fmol ($S/N=4$) [19] and 7.5 fmol/injection ($S/N=3$) [27,31]. The low detection limit of method enables the measurement of basal levels of urinary 8-OHdG in non-exposed healthy subjects that were not quantified in the previous report [27,31]. Furthermore, the analysis can be completed in 10 min and does not require washing and re-equilibrating the column, which makes it well suited for continuous analyses.

4. Conclusions

HILIC-MS/MS provides a selective, sensitive and rapid method for determining 8-OHdG in human urine. The method has acceptable linearity, accuracy, and precision, and is more sensitive than previously described LC–MS/MS methods that have been used in reversed-phase columns. The proposed HILIC–MS/MS method is well suited for large-scale human studies and clinical studies, and would also be applicable to analysis of 8-OHdG in not only urine but also other biological fluids such as plasma, serum and saliva, and in tissue.

Acknowledgements

This study was partly supported by the Industrial Technology Research Grant Program in 2005 from New Energy and Industrial Technology Development Organization (NEDO) of Japan (ID: 05A21705a), by a grant from the Smoking Research Foundation, and by a Grant-in-Aid for Scientific Research from the Ministry of Education, Culture, Sports, Science and Technology, Japan (21790126 and 23406004).

References

[1] J.G. Scandalios, Genome Biol. 3 (2002) 1019.1.
[2] J.E. Klaunig, L.M. Kamendulis, Annu. Rev. Pharmacol. Toxicol. 44 (2004) 239.
[3] P. Rossner Jr., V. Svecova, A. Milcova, Z. Lnenickova, I. Solansky, R.J. Sram, Mutat. Res. 642 (2008) 14.
[4] M.S. Cooke, M.D. Evans, M. Dizdaroglu, J. Lunec, FASEB J. 17 (2003) 1195.
[5] M.D. Evans, M. Dizdaroglu, M.S. Cooke, Mutat. Res. 567 (2004) 1.
[6] M.D. Evans, M.S. Cooke, Bioessays 26 (2004) 533.
[7] M.S. Cooke, M.D. Evans, R.M. Burd, K. Patel, A. Barnard, J. Lunec, P.E. Hutchinson, J. Invest. Dermatol. 116 (2001) 281.
[8] L.L. Wu, C.-C. Chiou, P.-Y. Chang, J.T. Wu, Clin. Chim. Acta 339 (2004) 1.
[9] K. Sakai, T. Ochi, M. Takeuchi, J. Anal. Bio-Sci. 32 (2009) 297.
[10] G. Guetens, G. De Boeck, M. Highley, A.T. van Oosterom, E.A. de Bruijn, Crit. Rev. Clin. Lab. Sci. 39 (2002) 331.
[11] H.E. Poulsen, S. Loft, H. Prieme, K. Vistisen, J. Lykkesfeldt, K. Nyyssonen, J.T. Salonen, Free Radic. Res. 29 (1998) 565.
[12] K. Shimoi, H. Kasai, N. Yokota, S. Toyokuni, N. Kinae, Cancer Epidemiol. Biomarkers Prev. 11 (2002) 767.
[13] J. Cadet, M. Berger, T. Douki, J.-L. Ravanat, Rev. Physiol. Biochem. Pharmacol. 131 (1997) 1.
[14] C. Tagesson, M. Källberg, C. Klintenberg, H. Starkhammar, Eur. J. Cancer 31A (1995) 934.
[15] J.-L. Ravanat, P. Guicherd, Z. Tuce, J. Cadet, Chem. Res. Toxicol. 12 (1999) 802.
[16] I. Holmberg, P. Stål, M. Hamberg, Free Radical Biol. Med. 26 (1999) 129.
[17] J.-L. Ravanat, B. Duretz, A. Guiller, T. Douki, J. Cadet, J. Chromatogr. B 715 (1998) 349.
[18] T. Renner, T. Fechner, G. Scherer, J. Chromatogr. B 738 (2000) 311.
[19] M.S. Cooke, R. Singh, G.K. Hall, V. Mistry, T.L. Duarte, P.B. Farmer, M.D. Evans, Free Radic. Biol. Med. 41 (2006) 1829.
[20] B. Crow, M. Bishop, K. Kovalcik, D. Norton, J. George, J.A. Bralley, Biomed. Chromatogr. 22 (2008) 394.
[21] B. Malayappan, T.J. Garrett, M. Segal, C. Leeuwenburgh, J. Chromatogr. A 1167 (2007) 54.
[22] F. Teichert, R.D. Verschoyle, P. Greaves, J.F. Thorpe, J.K. Mellon, W.P. Steward, P.B. Farmer, A.J. Gescher, R. Singh, Rapid Commun. Mass Spectrom. 23 (2009) 258.
[23] C.-W. Hu, C.-J. Wang, L.W. Chang, M.-R. Chao, Clin. Chem. 52 (2006) 1381.
[24] L. Sabatini, A. Barbieri, M. Tosi, A. Roda, F.S. Violante, Rapid Commun. Mass Spectrom. 19 (2005) 147.
[25] W.-Y. Hsu, W.T. Chen, W.-D. Lin, F.-J. Tsai, Y. Tsai, C.-T. Lin, W.-Y. Lo, L.-B. Jeng, C.-C. Lai, Clin. Chim. Acta 402 (2009) 31.
[26] A. Weimann, D. Belling, H.E. Poulsen, Nucleic Acids Res. 30 (2002) e7.
[27] M.S. Cooke, R. Olinski, S. Loft, Cancer Epidemiol. Biomarkers Prev. 17 (2008) 3.
[28] M.D. Evans, R. Olinski, S. Loft, M.S. Cooke, FASEB J. 24 (2010) 1249.
[29] A. Pilger, S. Ivancsits, D. Germadnik, H.W. Rüdiger, J. Chromatogr. B 778 (2002) 393.
[30] W. Jian, R.W. Edom, Y. Xu, N. Weng, J. Sep. Sci. 33 (2010) 681.
[31] A. Weimann, D. Belling, H.E. Poulsen, Free Radical Biol. Med. 30 (2001) 757.
[32] E.S. Grumbach, D.M. Wagrowski-Diehl, J.R. Mazzeo, B. Alden, P.C. Iraneta, LC GC North Am. 22 (2004) 1010.
[33] R.-I. Chirita, C. West, A.-L. Finaru, C. Elfakir, J. Chromatogr. A 1217 (2010) 3091.
[34] S. Drivelos, M.E. Dasenaki, N.S. Thomaidis, Anal. Bioanal. Chem. 397 (2010) 2199.

Environmental Science & Technology

Article

pubs.acs.org/est

Emission and Atmospheric Transport of Particulate PAHs in Northeast Asia

Yayoi Inomata,*[,†] Mizuo Kajino,[‡,§] Keiichi Sato,[†] Toshimasa Ohara,[∥] Jun-Ichi Kurokawa,[∥,†] Hiromasa Ueda,[⊥] Ning Tang,[#,$] Kazuichi Hayakawa,[#] Tsuyoshi Ohizumi,[†] and Hajime Akimoto[†]

[†]Asia Center for Air Pollution Research, 1182, Sowa, Nishi-ku, Niigatashi, Niigata, 950-2144, Japan

[‡]Meteorological Research Institute, 1-1, Nagamine, Tsukuba, Ibaraki, 305-0052, Japan

[§]Pacific Northwest National Laboratory, P.O. Box 999, Richland, 99352 Washington, USA

[∥]National Institute for Environmental Studies, 16-2, Onogawa, Tsukuba, Ibaraki, 305-8506, Japan

[⊥]Toyohashi University of Technology, Toyohashi, Aichi, 441-8580, Japan

[#]Graduate School of Natural Science and Technology, Kanazawa University, Kakuma-machi, Kanazawa, 920-1154, Japan

[$]Hyogo College of Medicine, 1-1, Mucogawacho, Nishinomiya, Hyogo, 663-8501, Japan

Supporting Information

ABSTRACT: The emission, concentration levels, and transboundary transport of particulate polycyclic aromatic hydrocarbons (PAHs) in Northeast Asia were investigated using particulate PAH measurements, the newly developed emission inventory (Regional Emission inventory in ASia for Persistent Organic Pollutants version, REAS-POP), and the chemical transport model (Regional Air Quality Model ver2 for POPs version, RAQM2-POP). The simulated concentrations of the nine particulate PAHs agreed well with the measured concentrations, and the results firmly established the efficacy of REAS/RAQM2-POP. It was found that the PAH concentrations in Beijing (China, source region), which were emitted predominantly from domestic coal, domestic biofuel, and other transformations of coal (including coke production), were approximately 2 orders of magnitude greater than those monitored at Noto (Japan, leeward region). In Noto, the PAH concentrations showed seasonal variations; the PAH concentrations were high from winter to spring due to contributions from domestic coal, domestic biofuel, and other transformations of coal, and low in summer. In summer, these contribution were decrease, instead, other sources, such as the on-road mobile source, were relatively increased compared with those in winter. These seasonal variations were due to seasonal variations in emissions from China, as well as transboundary transport across the Asian continent associated with meteorological conditions.

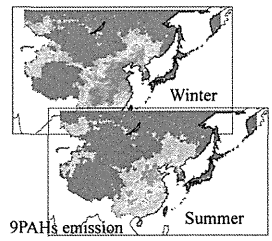

1. INTRODUCTION

Polycyclic aromatic hydrocarbons (PAHs) are highly carcinogenic to humans.[1] In general, PAHs are emitted from domestic, industrial, power plant, traffic, and open biomass burning sources during the incomplete combustion and pyrolysis of fossil fuels and biomass and during coke production.[2−4] China is one of the largest PAH-emitting countries in the world, and the high emission is associated with rapid economic and industrial growth.[3] High concentrations of PAHs were observed in Chinese urban sites.[5−7] Furthermore, comparatively high PAH concentrations have been observed at other locations in East Russia, South Korea, and Japan, which are related to the transboundary transport of PAHs from China.[5−7] PAHs originating from China have received increased attention as a potential human health risk in Northeast Asia.[8]

Although many measurements of particulate PAHs have been conducted,[5−7] these studies are insufficient to elucidate the pollution by PAHs in Northeast Asia. According to the European Monitoring and Evaluation Program (EMEP) project, which operates under the convention of long-range transboundary air pollution, transboundary transport and its contribution to the total deposition of PAHs is a significant source of POP pollution in Europe.[9] To evaluate the pollution levels and transboundary transport of PAHs in Northeast Asia, it is necessary to investigate the temporal and spatial variations of PAHs using a chemical transport model and a monitoring approach.

An inventory of PAH emissions is required to simulate PAH concentrations in the atmosphere. Until now, PAH emission inventories have been reported for several countries, such as the former Union of Soviet Socialist Republics, the European EMEP countries, the United States, and the United Kingdom.[10−13] In Asia, a few PAH emission inventories have been reported; Zhang and Tao reported the global inventory on a country basis.[3] The PAH emission inventory reported by Xu et al. and Zhang et al. focused on China only.[2,14] There is no available grid-based PAH emission inventory in Northeast Asia. Although the outflow of PAHs from China has been reported with the use of China's emission inventory,[15−17] a comprehensive view has not yet been obtained.

Received: October 20, 2011
Revised: March 19, 2012
Accepted: March 22, 2012
Published: March 22, 2012

dx.doi.org/10.1021/es300391w | Environ. Sci. Technol. 2012, 46, 4941−4949

To investigate the transboundary transport of particulate PAHs in Northeast Asia, measurements have been taken at several monitoring stations by a PAH-monitoring network in Northeast Asia that was established by a group at Kanazawa University under several projects, one of which is the "Study on potential threat caused by organic pollutants in the Japan Sea region".[5−7] In the present study, the spatial and temporal distributions of particulate PAH concentrations were investigated using our newly developed PAH emission inventory for Northeast Asia, applying the Regional Emission inventory in ASia (REAS) for Persistent Organic Pollutants version (REAS-POP),[18] and the Regional Air Quality Model ver2 for Persistent Organic Pollutants (RAQM2-POP) we developed.[19] The REAS/RAQM2-POP was verified by comparing the measured and simulated particulate concentrations for 9 PAHs (Flu, Pyr, BaA, Chr, BbF, BkF, BaP, IcdP, and BghiP) at the Beijing (China, source region) and Noto (Japan, approximately several thousand kilometers leeward from the eastern coast of China) monitoring sites.

2. MATERIALS AND METHODS

2.1. Emission Inventory. We developed the first gridded emission inventory of PAHs, the Regional Emission inventory in ASia for Persistent Organic Pollutants version (REAS-POP), in Northeast Asia. This method of estimating emissions is shown in Figure S1 in the Supporting Information (SI). The REAS-POP includes emission data for 16 PAHs (2 rings: naphthalene (NaP); 3 rings: acenaphthylene (Acy), acenapthene (Ace), fluorene (Flo), phenanthrene (Phe), and anthracene (Ant); 4 rings: fluoranthene (Flu), pyrene (Pyr), benz[*a*]anthracene (BaA), and chrysene (Chr); 5 rings: benzo[*b*]fluoranthene (BbF), benzo[*k*]fluoranthene (BkF), benzo[*a*]pyrene (BaP), and dibenz[*a,h*]anthracene (DahA) and 6 rings: indeno[1,2,3-*cd*]pyrene (IcdP) and benzo[*g,h,i*]perylene (BghiP)) that are listed as priority pollutants by the United States Environmental Protection Agency (USEPA).[20] The available measurement data used to validate REAS-POP was limited to 9 PAHs (Flu, Pyr, BaA, Chr, BbF, BkF, BaP, IcdP, and BghiP) because volatile PAHs that contain 2 or 3 rings could not be recovered by collecting airborne particulates. Therefore, the emission inventory in this study was focused on these 9 PAHs.

The monthly emission of each PAH species was estimated by following equation.

$$E_{(i)} = FC_d \times EF_{(i)} \times MF + FC_{nd}/12 \times EF_{(i)} + TR/12 \times EF_{(i)} + E_{BC} \times EF_{(i)/BC}$$

where

E is the each PAH emission (mg mon^{-1});
(i) is the PAH species;
FC_d is the fuel consumption rate for the domestic sector by REAS (mg yr^{-1});[18]
EF is the emission factor of each PAH (mg kg^{-1} or mg km^{-1});
MF is the grid-based monthly factor;[21,22]
FC_{nd} is the fuel consumption rate for sectors other than the domestic one by REAS (mg yr^{-1});[18]
TR is the traffic fuel consumption rate for on-road mobile sources by REAS (km yr^{-1});[18]
E_{BC} is the monthly black carbon (BC) emission of open biomass burning (mg mon^{-1}) from the Global Fire Emissions Database version 3 (GFEDv3);[23]
$EF_{(i)/BC}$ is the ratio of each PAH emission (mg) against BC emission (mg) by open biomass burning.

The PAH emissions are gridded at 0.5° × 0.5°, and these were interpolated into the model grids with a 60 × 60 km resolution. The period is from 2000 to 2005.

We describe the details of fuel and traffic fuel consumption rates by REAS, the emission factors, and the emission from open biomass burning in the following sections.

2.1.1. Annual Fuel Consumption Rates by REAS and Monthly Factors. Fuel consumption rates were derived from the Regional Emission inventory in ASia (REAS).[18] The fuel consumption rate was estimated at the province and country levels and was divided into a 0.5° × 0.5° grid by using several databases, including population data, information on the positions of large point sources, a land cover data set, and a land area data set.[18]

The fuel consumption rates were classified into two sources, stationary and on-road mobile sources. The fuel consumption rates of the stationary sources were classified into the following five economic sectors: domestic, industry, other transformation, power plant, and others. The fuel consumption rates of these stationary sources were also categorized by the following seven fuel types: coal (hard coal, brown coal, and derived coal (coke oven)), gas (natural gas), light fuel (motor gasoline and kerosene), diesel oil, heavy fuel (heavy fuel oil and crude oil), biofuel (fuel wood, crop residue, and animal waste), and others (municipal waste and charcoal). It is noted that coke and aluminum production, which are considered to be the sources of PAHs, are classified into "other transformation of coal" and "coal industry", respectively. Furthermore, the traffic fuel consumption rates of the on-road mobile sources were classified into seven types (light-duty gasoline vehicles, heavy-duty gasoline vehicles, light-duty diesel vehicles, heavy-duty diesel vehicles, gasoline buses, diesel buses, and motorcycles).

These fuel consumption rates were based on the annual average value. To estimate the monthly fuel consumption rate, usage of the space-heating component of residential energy was divided into monthly values because the space-heating component of residential energy use depends on the outdoor temperature. The MF was estimated using the ratio of monthly usage of the space-heating component of residential energy to the annual one.[21,22]

2.1.2. PAH Emission Factors. The factors affecting the emission of gas and particulate PAHs in Northeast Asia were collected from the literature (SI Table S1, S2, S3).[2,12,14,20−43] It was reported that emission factors varied widely depending on the combustion conditions (e.g., temperature, water content, and fuel type).[34] In addition, the data for emission factors for each source in this study was very limited; the number of emission factors for each source was in the range of 1−25. Therefore, the adopted emission factors included great uncertainty. We have attempted to perform sensitivity calculations using the maximum, minimum, and median values of the emission factors (see Section 3.3). The median values of emission factors were adopted in this study. If there were no available data for Northeast Asia on the emission factors of any of the sources, typical values from other parts of the world were adopted.[12] For the sources that had no information regarding the emission factors, the emission factors were considered to be 0.

2.1.3. PAH Emission from Open Biomass Burning by GFEDv3. PAH emission from open biomass burning was estimated using the burned area, the BC emission rate, and the

PAH and BC emission factors. The burned area and the BC emission rate were derived from GFEDv3, with a spatial resolution of 0.5° × 0.5° latitude/longitude and a monthly time resolution.[23] The burned area was classified into two types according to the land use categories in GFEDv3, agricultural waste burning and forest fire-type burning, based on the United States Geological Survey (USGS) land use data. The BC emission factor from open biomass burning was set to the median value (0.66 g kg^{-1}) of the available data set.[44−46] The emission factor of PAHs from BC emission was also determined to be the median value of the data set (SI Table S4).[34,40]

2.2. Off-line Coupled Meteorology (WRF)-Chemical Transport Model (RAQM2-POP). The Regional Air Quality Model ver2 for Persistent Organic Pollutants (RAQM2-POP)[19], aerosol chemical transport model, was used to simulate the PAHs. This model was used to investigate the long-range transport and deposition of sulfate, nitrate, and dust particles over Northeast Asia.[48−50] We developed RAQM2 to simulate the emission, long-range transport, and dry/wet deposition in particulate and gaseous phase PAHs. In RAQM2-POP, several processes such as advection, turbulent diffusion, aerosol dynamics (nucleation, condensation/evaporation, coagulation), partitioning between the gaseous and particulate phase, dry/wet deposition in particulate and gaseous phase, and degradation in the atmosphere were considered (SI Table S5). These specific parameters were almost the same as those used in the Meteorological Synthesizing Center-East (MSCE)-POP model, developed by MSC-E for the European Monitoring and Evaluation Programme (EMEP) region,[51] except aerosol dynamics and cloud microphysical processes. The PAH boundary condition was set to 0, because China is considered to be the dominant emission country. The specifics of RAQM2-POP have been described by Kajino et al.[19]

The Weather Research and Forecasting model version 3.0 (WRF) was used to provide the meteorological field for RAQM2-POP.[52] The National Centers for Environmental Prediction (NCEP) final operational analysis data (FNL), ds083.2 (http://dss.ucar.edu/data sets/ds083.2), were used to provide the initial and boundary conditions for WRF (http://dss.ucar.edu). The WRF and RAQM2-POP model domains cover most areas of the Northeast Asian countries. The horizontal grid resolution is 60 km with a Lambert conformal map projection, and there are 27 vertical layers from the ground surface to 100 hPa for WRF and 12 layers from the ground to 10 km (at approximately 50, 150, 300, 500, 750, 1500, 2500, 3500, 4500, 6000, 7500, and 8950 m) for RAQM2-POP. Emissions, concentrations, wet depositions, and dry depositions were output on an hourly basis.

2.3. Aerosol Observation and Chemical Analysis. The measurement of particulate PAH concentrations was conducted at two monitoring sites in Beijing (China, Longitude 116.4°E, Latitude 40.0°N) and Noto (coastal site on the Sea of Japan in Japan, Longitude 136.9°E, Latitude 37.5°N). These concentrations were used to validate the REAS/RAQM2-POP. Under prevailing westerly winds over midlatitudes, Beijing is considered to be the source monitoring site, and Noto is considered to be the leeward monitoring site.

At the Beijing monitoring site, sampling was conducted on the rooftop of a three-story building at the Chinese Academy of Sciences, Center for Ecological Research, which is located in Chaoyang District, during the period from 8 March 2005 to 13 April 2005 and from 10 May 2005 to 26 May 2005 at 1-day intervals. The Noto monitoring site is located on the Japanese main island (2.1 km downwind from the coastal line) in the Noto peninsula on the coast of the Sea of Japan. Airborne particulate matter was collected continuously from 31 December 2004 to 28 December 2005 at 1-week intervals. There were no major PAH emission sources around the Noto monitoring site. At both sites, the airborne particulate matter was collected on quartz-fiber filters (2500QAT-UP, Pallflex Products, Putnam, CT) using high-volume air samplers (Beijing, HV-1000F, Shibata, Japan; Noto, AH-600, Shibata, Japan).

Nine particulate PAHs (Flu, Pyr, BaA, Chr, BaP, BbF, BkF, BghiP, IcdP) were analyzed by HPLC with fluorescence detection at Kanazawa University. The details of the sampling and analysis have been described previously.[6,53]

3. RESULTS AND DISCUSSION

3.1. Emission of 9 PAHs in Northeast Asia. Figure 1 shows the geographical distribution of the annual emissions of the 9 PAHs at a resolution of 0.5° × 0.5° in Northeast Asia in 2005 (RAQM2-simulated domain; longitude 84−161°E, latitude 16−55.5°N). China was shown to be the most significant contributor of the 9 PAH contaminants in Northeast Asia. In particular, elevated levels of the 9 PAHs were noted in the North China Plain, the East coast of China, Guizhou, Sichuan Basin, and Northeastern China. The estimated annual emission of the 9 PAHs in China in 2005 was approximately 9.6 Gg yr^{-1} (1.3 mg m^{-2} $year^{-1}$), which accounted for 92% of the total emissions (10.5 Gg yr^{-1}) in Northeast Asia in 2005. According to a previous report,[2] the total emission of the 9 PAHs in China in 2003 was estimated to be 7.1 Gg yr^{-1}. This estimation was close to ours (8.0 Gg yr^{-1}) for 2003. The emission from the eastern part of Russia (East Russia) was estimated to be 0.19 Gg yr^{-1} (0.13 mg m^{-2} $year^{-1}$, 1.8% of the total emission of the 9 PAHs in Northeast Asia); North Korea, 0.29 Gg yr^{-1} (1.7 mg m^{-2} $year^{-1}$, 2.7%); Mongolia, 0.021 Gg yr^{-1} (0.014 mg m^{-2} $year^{-1}$, 0.20%); Japan, 0.020 Gg yr^{-1} (0.029 mg m^{-2} $year^{-1}$, 0.19%); South Korea, 0.020 Gg yr^{-1} (0.13 mg m^{-2} $year^{-1}$, 0.29%); and Taiwan, 0.0028 Gg yr^{-1} (0.045 mg m^{-2} $year^{-1}$, 0.0036%).

The estimated emissions and percentages of each species to the total emission of the 9 PAHs in 2005 were as follows: 2.2 Gg yr^{-1} (21%) for Flu, 1.9 Gg yr^{-1} (18%) for Pyr, 0.90 Gg yr^{-1} (9%) for BaA, 0.93 Gg yr^{-1} (9%) for Chr, 1.4 Gg yr^{-1} (13%) for BaP, 1.4 Gg yr^{-1} (13%) for BbF, 0.52 Gg yr^{-1} (5%) for BkF, 0.59 Gg yr^{-1} (6%) for BghiP, and 0.75 Gg yr^{-1} (7%) for IcdP. The largest emission was that of Flu, which contains 4 benzene rings, followed by that of Pyr (4 rings), BbF (5 rings), and that of BaP (5 rings) (see SI Figure S2). The emission profiles reflect the emission patterns from China, which is the dominant PAH-emitting country in Northeast Asia. However, the emission sources of the 9 PAHs vary considerably from county to country. In China, the dominant PAH sources were domestic coal (47%), domestic biofuel (18%), and other coal transformations, including coke production (29%). Xu et al. also estimated that domestic biofuel, domestic coal, and coke production were the dominant sources of PAH emission in China in 2003.[2] Open biomass burning contributes 0.3% of China's emissions. In East Russia, North Korea, and Mongolia, domestic biofuel (4% for East Russia, 33% for North Korea, and 43% for Mongolia), domestic coal (28% for East Russia, 61% for North Korea, and 11% for Mongolia), and other coal transformations (37% for East Russia, 3% North Korea, and 4% for Mongolia) were also dominant sources. Furthermore, the emission from open biomass burning was also a large contributor in East Russia (31%) and Mongolia (38%).

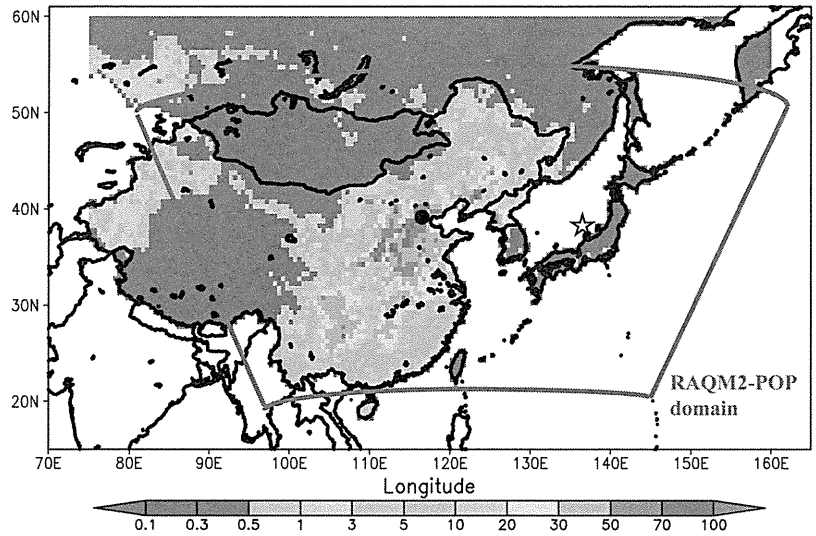

Figure 1. Spatial distributions of the annual emissions of 9 PAHs at a 0.5° × 0.5° resolution in 2005 in Northeast Asia by REAS-POP. The scale is in the units of mg yr^{-1} m^{-2}. ● indicates the location of Beijing, and ☆ indicates the location of Noto. The model domain used by RAQM2-POP is also shown.

In Japan and Taiwan, the major emission source was on-road mobile, accounting for 68% and 44% of the PAH emissions, respectively. These results are consistent with the results of the cluster analysis and factor analysis, which were based on the measurement data and demonstrated that the main source of PAHs in Japanese cities (Kanazawa, Tokyo, and Sapporo) was automobiles, especially diesel-engine vehicles.[5] The South Korean emissions originated primarily from on-road mobile sources (35%), industry (32%), other coal transformations (15%), and domestic coal (11%).

These PAH emissions, in this case BaP, show clear seasonal variation with high levels in winter to spring and low levels in summer (SI Figure S3a). The seasonal variation can be attributed to domestic coal and domestic biofuel sources because of the use of heating systems. Conversely, the relative contribution of the other coal transformations increased in summer (SI Figure S3b).

3.2. Evaluation of PAH Pollution in Northeast Asia.

3.2.1. Seasonal Variation of the Measured and Simulated PAH Concentrations at the Beijing and Noto Monitoring Sites. Figure 2 shows the comparison between the measured and simulated particulate PAH concentrations at the Beijing and Noto monitoring sites. At both sites, the simulated PAH concentrations generally agreed well with the measured concentrations. It was noted that the PAH concentrations measured in Beijing were 2 orders of magnitude greater than those measured in Noto.

At the Beijing monitoring site, the observed (simulated) average concentrations and the standard deviation of 6 PAHs were as follows: 6510 ± 6540 (7480 ± 5790) pg m^{-3} for Pyr, 6520 ± 5810 (5800 ± 3330) pg m^{-3} for Chr, 8100 ± 5890 (10100 ± 6940) pg m^{-3} for BbF, 3050 ± 2280 (2550 ± 1440) pg m^{-3} for BkF, 5790 ± 5060 (9250 ± 4350) pg m^{-3} for BaP, and 4250 ± 3070 (4440 ± 2210) pg m^{-3} for IcdP. The correlation coefficient for each species ranged from 0.30 to 0.58 (SI, Table S6). Pyr exhibits the highest concentration, which contains 4 benzene rings. The concentrations of PAHs gradually decreased from March to May. Additionally, the PAH concentrations in Beijing were characterized by daily variations. It is also noteworthy that the simulated PAH concentrations were significantly underestimated when measured concentrations were very high (15–16 March 2005 and 6 April 2005). Relatively higher concentrations were observed under weak wind speeds (data not shown), which causes weak dispersion of PAH concentrations in air. Furthermore, emission would also contribute to this discrepancy. In the RAQM2-POP, the emission was given as the monthly average value, and simulated concentrations were the average values on the grid (resolution 60 × 60 km), which cannot identify local sources on a daily basis. The large discrepancy between measurements and simulation would result from the contribution of the local source.

At the Noto monitoring site, the observed (simulated) average concentrations and standard deviations for the particulate 9 PAHs were as follows; 87.6 ± 77.2 (14.5 ± 21.9) pg m^{-3} for Flu, 60.8 ± 55.0 (11.5 ± 14.1) pg m^{-3} for Pyr, 14.1 ± 11.8 (47.8 ± 43.2) pg m^{-3} for BaA, 34.5 ± 26.3 (38.8 ± 35.3) pg m^{-3} for Chr, 44.9 ± 36.6 (34.3 ± 44.6) pg m^{-3} for BbF, 16.5 ± 12.2 (4.6 ± 5.7) pg m^{-3} for BkF, 23.5 ± 16.4 (13.1 ± 14.7) pg m^{-3} for BaP, 27.6 ± 17.6 (19.0 ± 16.2) pg m^{-3} for BghiP, and 21.3 ± 15.5 (4.74 ± 6.09) pg m^{-3} for IcdP (SI, Table S7). Although several simulated species, including Flu, Pyr, BkF, and IcdP, were underestimated, the seasonal variation (high in winter to spring and low in summer) is well reproduced by the simulation. The underestimation of several PAHs might be caused by the values set for several parameters such as degradation, dry/wet deposition during the long-range transport, and gas-particle partitioning. These parameters are subjects of future investigation. Compared with the source region (Beijing), the correlation coefficient of each PAH species between the measured and simulation values at Noto was high (0.73–0.87). One reason for this is that the measured concentrations at Beijing were strongly influenced by the emission from the local source. The large variation in concentrations was reduced due to the longer sampling time (1 week) at Noto. Furthermore, the higher correlation suggests that the variations in concentrations at remote sites such as Noto are mainly controlled by synoptic scale disturbances

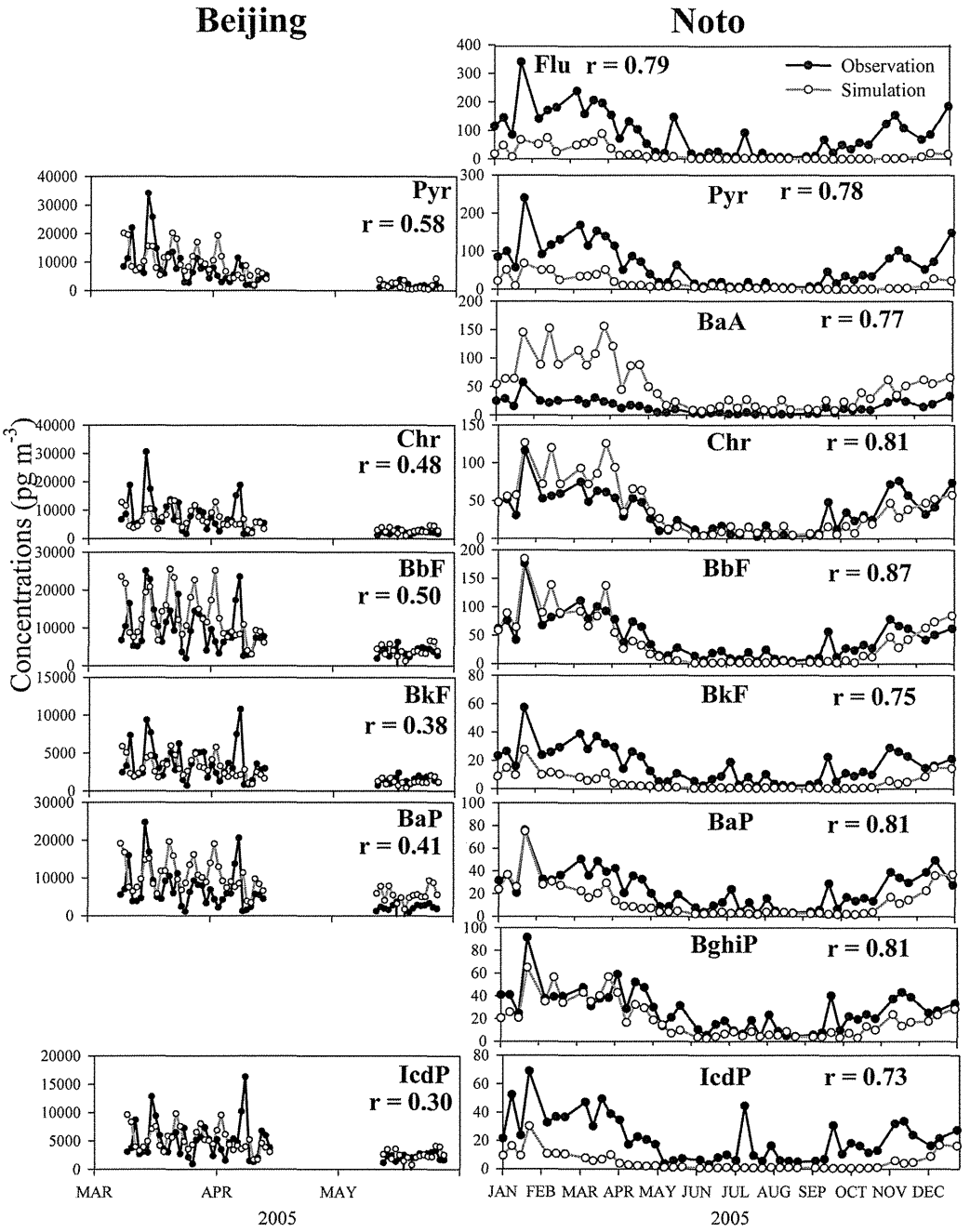

Figure 2. Comparison of the measured and simulated concentrations of the particulate 9 PAHs at Beijing (left panel) and Noto (right panel). The data at Beijing were a one-day average from March to May in 2005, whereas the Noto data were a weekly average from January to December in 2005. *r* is the correlation coefficient between the measured and simulated particulate concentrations.

(fronts, cyclones, and anticyclones), which are generally well predicted by regional-scale models.

These results also suggest that our newly developed REAS/RAQM2-POP is reasonably accurate in simulating the atmospheric particulate concentrations of 9 PAHs.

3.2.2. Spatial and Seasonal Variations in BaP Concentrations in Northeast Asia. Figure 3 shows the simulated temporal variation of BaP concentrations at the Noto monitoring site with these dominant sources. As shown in Figure 2, BaP concentrations showed clear seasonal variation with higher values in winter to spring and lower values in summer. The dominant source of BaP at Noto was domestic biofuel (11–18%), domestic coal (20–59%), and other transformation of coal (4–18%) from winter to spring. The contribution from domestic biofuel and coal combustion decreased toward summer, while the contribution from other sources was relatively increased. In particular, the contribution from the on-road mobile source was relatively higher in summer (10–17%).